HHS Public Access

Author manuscript

Cell Rep. Author manuscript; available in PMC 2022 October 04.

Published in final edited form as:

Cell Rep. 2022 September 13; 40(11): 111330. doi:10.1016/j.celrep.2022.111330.

Posttranslational S-nitrosylation modification regulates HMGB1 secretion and promotes its proinflammatory and neurodegenerative effects

Ru Yang[1], **Yun Gao**[1,2], **Hui Li**[1], **Wei Huang**[1], **Dezhen Tu**[1,2], **Mengnan Yang**[1], **Xingqian Liu**[1], **Jau-Shyong Hong**[2], **Hui-Ming Gao**[1,3,*]

[1]State Key Laboratory of Pharmaceutical Biotechnology, Ministry of Education Key Laboratory of Model Animal for Disease Study, Institute for Brain Sciences, Jiangsu Key Laboratory of Molecular Medicine, Model Animal Research Center, Medical School of Nanjing University, Nanjing, Jiangsu Province 210023, China

[2]Laboratory of Neurobiology, National Institutes of Health, National Institute of Environmental Health Sciences, Research Triangle Park, NC 27709, USA

[3]Lead contact

SUMMARY

Nuclear protein high-mobility group box 1 (HMGB1) can be actively secreted by activated immune cells and functions as a proinflammatory cytokine. Regulation of HMGB1 secretion is critical for treatment of HMGB1-mediated inflammation and related diseases. This study demonstrates that S-nitrosylation (SNO; the covalent binding of nitric oxide [NO] to cysteine thiols) by inducible nitric oxide synthase (iNOS)-derived NO at Cys106 is essential and sufficient for inflammation-elicited HMGB1 secretion. iNOS deletion or inhibition or Cys106Ser mutation prevents lipopolysaccharide (LPS)- and/or poly(I:C)-elicited HMGB1 secretion. NO donors induce SNO of HMGB1 and reproduce inflammogen-triggered HMGB1 secretion. SNO of HMGB1 promotes its proinflammatory and neurodegenerative effects. Intranigral HMGB1 injection induces chronic microglial activation, dopaminergic neurodegeneration, and locomotor deficits, the key features of Parkinson's disease (PD), in wild-type, but not Mac1 (CD11b/CD18)-deficient, mice. This study indicates pivotal roles for SNO modification in HMGB1 secretion and HMGB1-Mac1 interaction for inflammatory neurodegeneration, identifying a mechanistic basis for PD development.

Graphical Abstract

*Correspondence: gaohm@nju.edu.cn.

AUTHOR CONTRIBUTIONS

R.Y., Y.G., H.L., W.H., D.T., J.-S.H., and H.-M.G. designed the research; R.Y., Y.G., H.L., W.H., D.T., M.Y., and X.L. performed the research; R.Y., Y.G., H.L., W.H., D.T., and H.-M.G. analyzed the data; and R.Y. and H.-M.G. wrote the paper.

SUPPLEMENTAL INFORMATION

Supplemental information can be found online at https://doi.org/10.1016/j.celrep.2022.111330.

DECLARATION OF INTERESTS

The authors declare no competing interests.

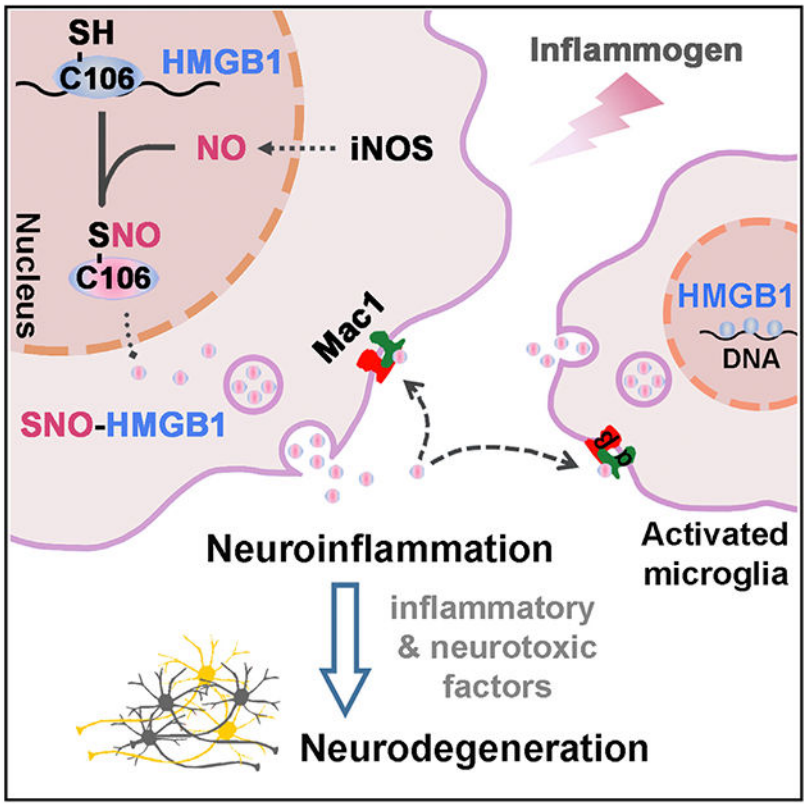

In brief

Regulation of HMGB1 secretion is critical for the treatment of HMGB1-mediated inflammation and related diseases. Yang et al. demonstrate that posttranslational S-nitrosylation modification (the covalent binding of nitric oxide to protein cysteine thiols) regulates HMGB1 secretion and promotes its proinflammatory and neurodegenerative effects, thereby contributing to Parkinson's disease pathogenesis.

INTRODUCTION

High-mobility group box 1 (HMGB1), a highly conserved DNA-binding protein, regulates gene transcription and genome stability within nuclei (Muller et al., 2004; Tang et al., 2011). HMGB1 can be passively released from necrotic cells and actively secreted from inflamed immune cells (e.g., macrophages, monocytes, and microglia). Once released, HMGB1 acts as a damage-associated molecular pattern (DAMP) or proinflammatory cytokine to initiate and perpetuate an inflammatory response (Gadani et al., 2015; Singh et al., 2016). Regulation of HMGB1 secretion is critical for the control of HMGB1-mediated inflammation and related diseases. Lacking a signal peptide, HMGB1 is secreted through endoplasmic reticulum-Golgi-independent unconventional secretory pathways (Gardella et al., 2002; Lu et al., 2014). Posttranslational lysine acetylation and serine phosphorylation within the two nuclear-localization sequences (NLSs; AA 28–44 and 180–185) of HMGB1 induced by the histone deacetylase inhibitor trichostatin A (TSA) and the PKC activator

phorbol 12-myristate 13-acetate (PMA), respectively, trigger HMGB1 secretion (Bonaldi et al., 2003; Elenkov et al., 2011; Youn and Shin, 2006). However, HMGB1 with acetylation- or phosphorylation-defective mutations (with replacement of lysines and serines to arginines and alanines, respectively) in the NLS is still secreted in response to TSA or PMA, respectively. TSA- and PMA-triggered secretion of such mutant HMGB1 is attenuated by the antioxidant N-acetyl cysteine. These findings suggest that acetylation and phosphorylation within the NLS are not indispensable for HMGB1 secretion and that oxidation participates in the regulation of HMGB1 secretion (Kwak et al., 2019). HMGB1 contains three cysteine residues (i.e., Cys23, Cys45, and Cys106) that are redox sensitive. Oxidation of Cys23 and Cys45 and formation of an intramolecular disulfide bond between them induces HMGB1 nucleocytoplasmic translocation and secretion (Kwak et al., 2019).

S-nitrosylation (SNO) is the covalent binding of nitric oxide (NO; a free radical gas) to a thiol of a cysteine residue to form S-nitrosothiol. SNO modulates wide-ranging functions and signaling events, such as transcriptional activity, mitochondrial function, enzymatic activity, synaptic plasticity, protein subcellular location, and cell death/survival, thereby playing important roles in human health and disease (Foster et al., 2009; Garbán et al., 2005; Hara et al., 2005; Rizza et al., 2018; Seth et al., 2018). Interestingly, aberrant protein SNO modification and proinflammatory effects of extracellular HMGB1 have been increasingly implicated in several seemingly diverse human diseases with redox imbalance and elevated inflammation as shared features, such as cancer, sepsis, cardiac ischemia/reperfusion injury, and neurodegenerative diseases (Andrassy et al., 2008; Benedet et al., 2018; Deng et al., 2018; Fauconnier et al., 2011; Gaikwad et al., 2021; Gdynia et al., 2016; Hotchkiss and Karl, 2003; Moldogazieva et al., 2018; Nakamura and Lipton, 2016; Sims et al., 2010; Wang et al., 1999). We previously showed that extracellular HMGB1 released from activated microglia and/or degenerating neurons served as a main mediator bridging chronic neuroinflammation and progressive neurodegeneration (Gao et al., 2011b). It is of special interest that environmental risk factors of Alzheimer's (AD), Parkinson's (PD), and Huntington's diseases (the three most common neurodegenerative diseases) exacerbate nitrosative stress and protein SNO modification via excessive NO production (Choi et al., 2014; Haun et al., 2013; Nakamura and Lipton, 2016; Nakamura et al., 2013, 2021). By directly modifying target proteins or forming reactive nitrogen species via further oxidation, NO functions as a key signaling molecule under physiological and pathophysiological conditions. During inflammation, NO, derived from inducible NO synthase (iNOS, also known as NOS2), reaches a high level (micromolar ranges) and serves as a major inflammatory mediator (Kapil et al., 2020; Liu et al., 2002; Yeh et al., 2011). It has become increasingly clear that many effects of NO are mediated by SNO (Foster et al., 2009; Nakamura and Lipton, 2016).

The present study investigated the regulation of posttranslational SNO modification on HMGB1 secretion and identified Cys106 as a key residue for secretion-linked SNO. Determination of the pathophysiological significance of SNO-linked HMGB1 secretion showed that S-nitrosylated HMGB1 (SNO-HMGB1) induced more profound microglial activation and neurodegeneration than unmodified HMGB1. Intranigral HMGB1 injection induced chronic microglial activation, dopaminergic neurodegeneration, and locomotor deficit (the key features of PD) in wild-type (WT) mice but not mice deficient in

macrophage antigen complex 1 (Mac1, also known as CR3, integrin αM/β2, and CD11b/CD18), indicating an important contribution of HMGB1-Mac1 interaction to the pathogenesis of PD.

RESULTS

NO-mediated secretion of HMGB1 from brain microglia/macrophages

Investigation of the regulatory mechanisms of HMGB1 secretion is pivotal for understanding the pathogenic roles of extracellular HMGB1 in various diseases related to HMGB1-mediated inflammation and for developing HMGB1-related anti-inflammatory therapeutics for these diseases. Here, we performed an intranigral injection of the inflammogen lipopolysaccharide (LPS) or saline into mice to examine how inflammation affected HMGB1 secretion from brain microglia. Microglia are the resident brain immune cells and are also known as brain parenchymal macrophages or brain-resident macrophages because of their multiple similarities. Because of a possible involvement of infiltrated peripherally derived monocytes/macrophages in results related to the intranigral injection and the difficulty in getting a clear distinction between brain microglia and peripheral macrophages, microglia/macrophages were used in the corresponding results description. At 24 h after the injection, amoeboid-like activated microglia/macrophages in LPS-injected substantia nigra (SN; the major pathological brain region in PD) displayed much weaker staining of nuclear HMGB1 (n-HMGB1) than ramified (resting) microglia/macrophages in saline-injected SN. No obvious cytosolic HMGB1 in activated microglia/macrophages indicated there was not a long cytosolic retention period of HMGB1 once its secretion mechanism was initiated (Figures 1A and 1B). As expected, CD11b-negative non-microglial brain cells (e.g., neurons and astroglia) in saline- and LPS-injected SN exhibited very strong n-HMGB1 staining (Figure 1A). Quantification of n-HMGB1 staining revealed a significant reduction in activated microglia/macrophages but not resting microglia/macrophages or non-microglial brain cells (Figure 1B). These *in vivo* results indicated that LPS triggered HMGB1 secretion from activated brain microglia/macrophages.

A remarkable increase in extracellular HMGB1 in the culture medium and significant reduction of intracellular HMGB1 in LPS-treated primary microglia confirmed extracellular secretion of HMGB1 from activated microglia (Figure 1C). A dramatic up-regulation of iNOS was observed in the lysate of LPS-treated microglia (Figure 1C). The positive association between HMGB1 secretion and iNOS upregulation hinted at a possible regulation of iNOS-derived NO on HMGB1 secretion. We next investigated whether NO regulated HMGB1 secretion. Prevention of LPS-elicited HMGB1 secretion by the iNOS-specific inhibitor 1400W indicated regulation of HMGB1 secretion by iNOS-derived NO (Figure 1C). Similarly, HMGB1 secretion from microglia-enriched cultures treated with another inflammogen, poly(I:C) (polyinosinic:polycytidylic acid; a synthetic dsRNA; 50 μg/mL), was also blocked by 1400W (data not shown). The NO donor sodium nitroprusside (SNP; 20 μM) triggered HMGB1 secretion from microglia (Figure 1C). Nuclear fractioning and immunoblotting analysis showed blockage of LPS-elicited HMGB1 secretion and n-HMGB1 reduction by 1400W (Figures 1D and 1E). Indeed, LPS and poly(I:C) induced production of NO in microglia-enriched cultures, which was blocked by 1400W. SNP

treatment also resulted in NO production (Figure 1F). No cytotoxicity in the MTT (3-[4,5-dimethylthiazol-2-yl]-2,5 diphenyl tetrazolium bromide) assay excluded the possibility that the observed effects of LPS, 1400W, SNP, or combined LPS and 1400W on HMGB1 secretion were attributable to microglial death from non-specific toxicity of these reagents (Figure 1G). These results together indicated that NO mediated HMGB1 secretion.

Genetic deletion of iNOS blocks LPS-induced HMGB1 secretion

iNOS catalyzes the oxidation of L-arginine to produce large amounts of NO and is a key mediator of inflammation (Kapil et al., 2020; Liu et al., 2002; MacMicking et al., 1997; Yeh et al., 2011). Different from the two constitutively expressed isoforms—neuronal NOS (nNOS) and endothelial NOS (eNOS)—that produce nanomolar amounts of NO, iNOS is expressed on inflammatory cells, endothelium, and epithelium during inflammation and produces micromolar amounts of NO for extended periods of time (Abu-Soud et al., 1997; Kapil et al., 2020; Kone et al., 2003; Liu et al., 2002; MacMicking et al., 1997; Sharma et al., 2007; Yeh et al., 2011). To further evaluate the dependence of HMGB1 secretion on iNOS-derived NO, we examined how iNOS deficiency affected HMGB1 secretion after LPS challenge. At 5 h after an intraperitoneal (i.p.) injection of LPS, serum HMGB1 was remarkably increased in WT mice but not $iNOS^{-/-}$ mice (Figures 2A and 2B). At 24 h after intranigral LPS injection, nigral microglia/macrophages in WT and $iNOS^{-/-}$ mice displayed similar amoeboid-like appearance and upregulation of the microglia/macrophage marker CD11b. In contrast to the remarkable HMGB1 secretion in activated WT microglia/macrophages, activated $iNOS^{-/-}$ microglia/macrophages failed to secrete HMGB1. The staining pattern of HMGB1 in activated $iNOS^{-/-}$ microglia/macrophages in LPS-injected SN was indistinguishable from that in resting microglia/macrophages in saline-injected SN of WT and $iNOS^{-/-}$ mice (Figures 2C and 2D). The complete blockage of HMGB1 secretion by iNOS deletion in these *in vivo* studies lends strong evidence for an essential role of iNOS-derived NO in the regulation of HMGB1 secretion under inflammatory conditions.

SNO modification of HMGB1 triggers its nucleocytoplasmic shuttling and extracellular secretion

Increasing evidence has indicated that many effects of NO are mediated by SNO, a posttranslational modification at cysteine thiols specifically mediated by NO. HMGB1 contains three cysteine residues. We next studied whether NO exerted its regulatory role in HMGB1 secretion through specific SNO modification of HMGB1. The overall level of SNO modification, which was detected by an antibody specific for S-nitroso-cysteine (SNO-C), was significantly increased in LPS-, poly(I:C)-, or SNP-treated primary microglia. The pretreatment with 1400W prevented LPS- or poly(I:C)-induced increase of SNO-C (Figures 3A and 3B). Notably, treatment of microglia with LPS, poly(I:C), or SNP led to the concurrence of cytosolic $SNO\text{-}C^{+}HMGB1^{+}$ staining with reduced n-HMGB1 staining that was negative for SNO-C staining (Figure 3A). Another NO donor, S-nitrosoglutathione (GSNO; 50 μM), produced results similar to those of SNP (data not shown). The pretreatment with 1400W prevented LPS- or poly(I:C)-induced elevation in cytosolic $SNO\text{-}C^{+}HMGB1^{+}$ immunostaining and reduction in n-HMGB1 staining (Figures 3A and 3B). These results together suggested that SNO modification of HMGB1 elicited its nucleocytoplasmic shuttling and extracellular secretion.

Results from immunoblotting analysis, immunoprecipitation, and biotin-switch assay further indicated that secreted HMGB1 in the medium of microglia/macrophage cultures treated with LPS, poly(I:C), and/or SNP was S-nitrosylated. iNOS inhibition by 1400W attenuated inflammogen-elicited secretion of SNO-HMGB1 (Figures 3C, 3D, 3F, 3G, and S1). First, in immunoblotting analysis, separated proteins were immunoblotted and probed for SNO-C and, after the blotting membrane was stripped, for HMGB1. As shown in Figure 3C, secreted HMGB1 in the concentrated medium of LPS-treated microglial cultures was S-nitrosylated, and 1400W lowered the level of extracellular SNO-HMGB1. Second, immunoprecipitated HMGB1 from the concentrated medium of LPS- or SNP-treated BV2 microglial cells was positive for SNO-C (Figure 3D). Third, biotin-switch assay was performed to specifically detect S-nitrosylated proteins in the concentrated culture medium. After free thiols were blocked by the thiol-specific methylthiolating agent methyl methanethiosulfonate (MMTS), nitrosothiol bonds were selectively decomposed with ascorbate to form thiols. Newly formed thiols were rapidly reacted with biotin-HPDP (N-[6-(biotinamido)hexyl]-3'-(2'-pyridyldithio)propionamide). Thus, S-nitrosylated cysteines were converted to biotinylated cysteines (Figure 3E). To detect biotinylated proteins, the same samples were loaded onto one non-reducing SDS-PAGE gel twice with the prestained protein marker in between. Separated proteins that contained biotinylated cysteines were immunoblotted and probed for biotin and, after the membrane was stripped, for HMGB1 or vice versa (Figure 3F). The result showed that secreted HMGB1 in the medium of poly(I:C)- or SNP-treated RAW 264.7 cells and LPS/poly(I:C)/SNP-treated peritoneal macrophages was S-nitrosylated and experimentally switched to biotin-HMGB1. 1400W greatly decreased the level of extracellular biotin-HMGB1 (Figures 3F, 3G, and S1). Thus, during LPS- or poly (I:C)-mediated inflammation, iNOS-derived NO S-nitrosylated HMGB1, thereby triggering its nucleocytoplasmic shuttling and extracellular secretion. The NO donor SNP/GSNO induced SNO of HMGB1 and reproduced inflammogen-elicited secretion of SNO-HMGB1. Collectively, posttranslational SNO modification of HMGB1 regulated its nuclear-to-cytoplasmic shuttling and extracellular secretion.

SNO modification of HMGB1 at Cys106 is required for its secretion

To more rigorously demonstrate the dependence of HMGB1 secretion on its SNO modification and to further determine the key cysteine residue(s) responsible for secretion-linked SNO modification, we constructed a recombinant pCS2(+)-4HA-HMGB1 plasmid and performed site-directed mutagenesis. With rising awareness of the necessity of the utilization of immune cells, especially primary immune cells, to investigate immune functions, we co-transfected freshly prepared mouse peritoneal macrophages with plasmids pCS2(+)-4HA-HMGB1 and pLVX-GFP, although it would be much easier to conduct plasmid transfection in currently widely used non-immune cell lines. Indeed, as the first line of defense against pathogen invasion, macrophages are very difficult to transfect with plasmids/viruses without affecting their survival and immune/inflammatory activity. We screened several transfection reagents and optimized the transfection procedure to achieve ~60% transfection efficiency without cytotoxicity during a 48 h plasmid transfection in peritoneal macrophages. We quantified fluorescence intensity of hemagglutinin (HA) immunostaining in macrophages expressing both GFP and HA-HMGB1. This method better discriminated non-transfected cells from the cells whose nuclear HA-HMGB1 was

"emptied" and whose cytosolic HA staining was weak after LPS/SNP treatment, which resulted from the extracellular secretion of HA-HMGB1.

WT and various mutant (C23S, C45S, C106S, and C23SC45 SC106S) HA-HMGB1 displayed nuclear localization in vehicle-treated macrophages. LPS/SNP treatment resulted in dramatic decreases in nuclear and total intracellular WT HA-HMGB1 and a mild increase in cytosolic WT HA-HMGB1 in macrophages. These results, combined with the treatment-elicited distinctive staining pattern change of WT HA-HMGB1, from nuclear staining in vehicle-treated macrophages to ring-like cytosolic staining in LPS- or SNP-treated macrophages, supported the occurrence of the extracellular secretion of WT HA-HMGB1 after its nucleus-to-cytoplasm shuttling but did not support completely cytosolic retention without extracellular secretion. In striking contrast to the remarkable secretion of WT HA-HMGB1 triggered by LPS/SNP, C106S mutant HA-HMGB1 was retained in the nucleus after the same treatment, and C106S mutation prevented LPS- or SNP-induced reduction in intracellular WT HMGB1 (Figures 4A and 4B). Similarly, C23SC45SC106S mutation blocked LPS- and SNP-elicited nucleocytoplasmic shuttling and secretion of HA-HMGB1 (Figures 4C and S2A). However, C23S or C45S mutation did not impair SNP- or LPS-triggered HA-HMGB1 shuttling and secretion (Figures 4C, S2B, and S2C). The complete prevention of LPS-triggered HMGB1 secretion by C106S and C23SC45SC106S mutations but not by C23S or C45S mutation in peritoneal macrophages indicated that SNO modification at Cys106 by iNOS-derived NO was essential and sufficient for HMGB1 secretion during inflammation.

SNO-HMGB1 induces more profound microglial activation and neurodegeneration than unmodified HMGB1

We next determined the pathophysiological significance of SNO-mediated HMGB1 secretion in the experimental setting of PD. Considering the essential role of iNOS-derived NO in SNO modification and secretion of HMGB1, we first examined how iNOS inhibition affected neurodegeneration. Pretreatment of midbrain neuron-glia cultures with 1400W prevented LPS- or poly(I:C)-induced neurodegeneration that was indicated by significant reductions in the levels of neuron-specific nuclear protein (Neu-N; a neuronal marker), PSD95 (a postsynaptic scaffold protein that is widely used to evaluate synapse damage), and tyrosine hydroxylase (TH; a marker of dopamine neurons) 7 days after LPS or poly(I:C) treatment (Figures 5A and 5B). Neuroprotection by 1400W in neuron-glia cultures (Figures 5A and 5B), or by 4-week infusion of 1400W and the NADPH oxidase inhibitor diphenyleneiodonium in a two-hit mouse model of PD involving both genetic and inflammatory insults (Gao et al., 2011a), indicated a crucial contribution of iNOS-derived NO to inflammatory neurodegeneration.

We next determined the pathophysiological significance of SNO-mediated HMGB1 secretion. SNO-HMGB1 (250 ng/mL), generated by *in vitro* SNO modification of endotoxin-free recombinant HMGB1 by the NO donor GSNO, induced microglial activation, neuronal death, and dendrite degeneration in neuron-glia cultures after a 7-day treatment (Figures 5C–5F). After treatment with SNO-HMGB1, neuron-glia cultures displayed significant increases in microglial number and expression of ionized

calcium binding adapter molecule 1 (Iba1; a microglia/macrophage marker) as well as significant decreases in neuronal number and Neu-N level. Moreover, immunostaining for microfilament-associated protein-2 (MAP-2; a neuron-specific protein with a function of microtubule stabilization in dendrites of postmitotic neurons) detected dendrite degeneration after SNO-HMGB1 treatment. Unmodified HMGB1 (250 ng/mL) or "incubated GSNO" (<5 μM after possible decomposition during 1-h incubation at 37°C in the *in vitro* SNO reaction and 1:10 dilution when added to the culture) did not induce microglial activation or neuronal loss (Figures 5C–5F). Therefore, SNO-HMGB1 induced more profound microglial activation and neurodegeneration than unmodified HMGB1.

Our previous findings showed that neutralization of HMGB1 rescued dopamine neurons from chronic degeneration induced by LPS, 1-methyl-4-phenylpyridinium, and the pesticide rote-none, three toxins often used to create models of PD. Treatment with HMGB1 (400 ng/mL) for 7 days induced dopaminergic neurodegeneration only in neuron-glia cultures and not in neuron-enriched cultures. Further mechanistic studies indicated that HMGB1 bound to the microglial surface receptor Mac1 (a pattern recognition receptor expressed in myeloid-lineage cells, including peripheral macrophages and brain microglia) and that the HMGB1-Mac1-NADPH oxidase signaling axis bridged chronic neuroinflammation and progressive neurodegeneration (Gao et al., 2011b). SNO modulates the functions of target proteins by changing their activity or interactions with other proteins (Hess et al., 2005; Stamler and Meissner, 2001). In the present study, we found that neuron-glia cultures generated from $Mac1^{-/-}$ mice were more resistant to unmodified HMGB1 and SNO-HMGB1 than cultures from WT mice. At 250 ng/mL concentration, while unmodified HMGB1 was "non-toxic" to both WT and $Mac1^{-/-}$ cultures, SNO-HMGB1 induced chronic neurodegeneration in WT cultures but not $Mac1^{-/-}$ cultures (Figure 6). The resistance of $Mac1^{-/-}$ neuron-glia cultures to unmodified and S-nitrosylated HMGB1, the stronger proinflammatory and neurodegenerative effects of SNO-HMGB1 compared with unmodified HMGB1 (Figures 5 and 6), and the binding of unmodified HMGB1 to microglial Mac1 demonstrated by co-immunoprecipitation and a direct binding analysis of membrane fractions of WT but not $Mac1^{-/-}$ microglia with recombinant HMGB1 protein (Gao et al., 2011b), together suggested that SNO-HMGB1 also bound to Mac1 with higher affinity than unmodified HMGB1. At 400 ng/mL concentration, unmodified HMGB1 induced neurodegeneration in WT but not $Mac1^{-/-}$ cultures, which confirmed our previous findings (Gao et al., 2011b). SNO-HMGB1 (400 ng/mL) caused neurodegeneration even in $Mac1^{-/-}$ cultures, but neurodegeneration was more severe in WT cultures than in $Mac1^{-/-}$ cultures (Figure 6). These results suggested the involvement of other receptors in HMGB1-mediated neurotoxicity, especially at high concentrations and after SNO modification. In summary, our findings uncovered a pivotal role for SNO modification in active secretion of HMGB1 from activated microglia/macrophages and revealed stronger proinflammatory and neurodegenerative effects of extracellular SNO-HMGB1 than unmodified HMGB1.

Intranigral HMGB1 injection induces microglial activation, dopaminergic neurodegeneration, and locomotor deficit in WT but not $Mac1^{-/-}$ mice

Multiple lines of evidence, including ours in this study, have indicated that posttranslationally modified HMGB1 can be actively secreted from activated immune cells

and serve as a proinflammatory cytokine to promote existing inflammation. Extracellular unmodified HMGB1, passively released from necrotic cells, can act as a DAMP to alert immune cells and to initiate non-infectious inflammation. We next conducted an intranigral injection of unmodified HMGB1 in WT and Mac1$^{-/-}$ mice to further examine whether HMGB1-elicited inflammatory neurodegeneration induces PD-like behavior deficits and to better elucidate the role of Mac1 in mediating HMGB1's effects in *in vivo* studies. Because the *in vitro* data revealed stronger proinflammatory and neurodegenerative effects of SNO-HMGB1 than of unmodified HMGB1 (Figures 5 and 6) and both had pathological relevance, we chose to inject unmodified HMGB1 rather than SNO-HMGB1. As shown in Figures 7A and 7B, HMGB1 injection induced microglia/macrophage activation and dopaminergic neurodegeneration in the SN of WT mice but not Mac1$^{-/-}$ mice at 1 month after the injection. HMGB1-injected SN of WT mice displayed a mild and chronic neuroinflammation, as indicated by increased immunoreactivity of Iba1, CD11b, and TMEM119 in microglia and their morphological changes from a ramified resting shape to an active appearance with irregular and enlarged cell body. TMEM119 is a newly developed specific microglial marker and is not expressed by peripheral macrophages or other immune/brain cells. Microglia/macrophages in HMGB1-injected SN of Mac1$^{-/-}$ mice and saline- or bovine serum albumin (BSA)-injected SN of WT and Mac1$^{-/-}$ mice exhibited the ramified resting morphology (Figures 7A and 7B) or no CD11b staining in Mac1$^{-/-}$ mice (data not shown). Immunohistochemistry and cell count showed significant reduction in the number of nigral TH-immunoreactive (IR) dopamine neurons in WT but not Mac1$^{-/-}$ mice at 1 month after intranigral HMGB1 injection. BSA injection did not cause detectable dopaminergic neurodegeneration (Figures 7A and 7B).

A rotarod test revealed locomotor impairment in HMGB1-injected WT mice but not HMGB1- or BSA-injected Mac1$^{-/-}$ mice at 1 month after the intranigral injection (Figure 7C). No significant difference in the duration or the distance traveled in the center zone in the open field test indicated no anxiety-related activity or impairment in exploratory activities in HMGB1- or BSA-injected WT or Mac1$^{-/-}$ mice (Figure 7D). Collectively, *in vivo* and *in vitro* findings indicated that both unmodified HMGB1 and SNO-HMGB1 were able to activate microglia, inducing inflammatory neurodegeneration. HMGB1-elicited inflammatory neurodegeneration caused PD-like locomotor deficit in WT mice. The resistance of Mac1$^{-/-}$ mice to HMGB1 injection (Figure 7) and Mac1$^{-/-}$ neuron-glia cultures to SNO-HMGB1 treatment (Figure 6), along with Mac1 expression in microglia but not neurons/astroglia in the brain and the requirement of microglia for HMGB1-mediated neurodegeneration (Gao et al., 2011b), indicated a pivotal role for microglial Mac1 receptor in HMGB1's proinflammatory and neurodegenerative effects.

DISCUSSION

The present study uncovered a pivotal role for SNO modification by iNOS-derived NO in HMGB1 secretion and its proinflammatory and neurodegenerative effects and further identified Cys106 as an essential residue for secretion-linked SNO. Determination of the pathological significance of secretion-linked SNO of HMGB1 in experimental settings of PD revealed that SNO-HMGB1 induced more profound microglial activation and neurodegeneration than unmodified HMGB1 through increased binding to microglial Mac1.

One month after intranigral HMGB1 injection, WT but not Mac1$^{-/-}$ mice displayed chronic microglial activation, dopaminergic neurodegeneration, and locomotor deficit, indicating an important contribution of HMGB1-Mac1 interaction to PD pathogenesis.

Nitrosative stress and oxidative stress are two intertwined key pathologic factors in many chronic diseases, including neurode-generative diseases. In situations associated with production of excessive reactive oxygen species (ROS) and dominant oxidative stress without or before induction of iNOS and production of a sufficient amount of NO for preferential SNO, oxidation plays a critical regulatory role in HMGB1 secretion. Such situations often occurred in some experimental settings for studying HMGB1 nucleocytoplasmic translocation with further investigation of its intracellular functions (e.g., autophagy and nuclear transport) or its extracellular secretion, as exemplified by non-immune cells (e.g., HEK293T, CHO, Panc2.03 tumor cell line, and primary/immortalized mouse embryonic fibroblasts [MEFs]), oxidative stimuli (e.g., H_2O_2, glucose oxidase, mitochondrial inhibitors, diamide, and starvation), and/or HEK293-hTLR4/MD2/CD14 cells expressing WT or Cys mutant HMGB1-EGFP with LPS treatment for 2 h (Hoppe et al., 2006; Kwak et al., 2019; Tang et al., 2010). It has been reported that H_2O_2-induced oxidation of Cys23 and Cys45 and formation of an intramolecular Cys23–Cys45 disulfide bond trigger HMGB1 secretion. Such effects are mediated by H_2O_2-eliminating enzyme peroxiredoxins that reduce H_2O_2 with thiols of cysteine residues (Kwak et al., 2019). Interestingly, compared with Cys23 and Cys45, Cys106 of HMGB1 is relatively less susceptible to oxidative modification. Free thiols of Cys106 and the Cys23–Cys45 disulfide bond of HMGB1 are detected in whole-cell lysates of HEK293T and CHO cells exposed to oxidative stimulation, supernatants of THP-1 cells challenged with 6 h LPS stimulation or freeze-thaw cycles for mechanical necrotization, and supernatants of macrophages subjected to freeze-thaw cycles or pyroptotic induction with ATP, monosodium urate, or aluminum (Hoppe et al., 2006; Kwak et al., 2019; Lu et al., 2012; Venereau et al., 2012). Because no NO is produced under these experimental settings (Gross et al., 2014), it is not a surprise to detect free thiol but not S-nitrosothiol at Cys106 of HMGB1.

In contrast to the seemingly inappreciable involvement of Cys106 in HMGB1 oxidation and oxidation-linked HMGB1 secretion, SNO of Cys106 was indispensable for NO-related regulation of HMGB1 secretion. The blockage of inflammation-elicited HMGB1 secretion by iNOS deletion in *in vivo* studies and by iNOS inhibitor in cultured microglia/macrophages (Figures 1 and 3) indicated an essential role of iNOS-derived NO in the regulation of HMGB1 secretion under inflammatory conditions. Secreted HMGB1 in the culture medium and cytosolic HMGB1 redirected from nuclei of LPS/poly(I:C)/SNP-treated microglia/macrophages, but not n-HMGB1, exhibited SNO modification (Figure 3). Furthermore, prevention of LPS- or poly(I:C)-elicited SNO by iNOS inhibition blocked HMGB1 secretion (Figure 3), indicating that SNO modification by iNOS-derived NO was a key regulatory mechanism of HMGB1 secretion. The complete prevention of LPS-triggered HA-HMGB1 secretion by C106S and C23SC45SC106S mutations but not by C23S or C45S mutation in peritoneal macrophages (Figure 4 and S2) indicated that SNO modification at Cys106 by iNOS-derived NO was essential and sufficient for active HMGB1 secretion during inflammation. Because the NO donor SNP only provides NO and cannot cause other posttranslational modifications on HMGB1 except SNO (Figure 3), the prevention of

SNP-triggered HA-HMGB1 secretion by C106S and C23S C45SC106S mutations but not C23S or C45S mutation (Figures 4 and S2) further supported the idea that SNO at Cys106 mediated HMGB1 secretion. Taken together, SNO modification at Cys106 was essential and sufficient for active HMGB1 secretion from microglia/macrophages.

To determine whether there was cross-regulation between oxidation and SNO in regulating HMGB1 secretion, we examined how genetic deletion of gp91 (the catalytic subunit of NADPH oxidase) affected LPS- or SNP-elicited HMGB1 secretion in the absence or presence of 1400W. NADPH oxidase is a major source of ROS production during inflammation and has been implicated as a novel therapeutic target for neurodegenerative diseases (Gao et al., 2012). Deficiency of gp91 did not significantly alter LPS- or SNP-induced HMGB1 secretion. 1400W blocked LPS-induced HMGB1 secretion in both WT and $gp91^{-/-}$ microglia (Figure S3). These results indicated that HMGB1 secretion from activated microglia was mediated by iNOS-derived NO, independent of NADPH oxidase-derived ROS. Moreover, after the biotin-switch reaction that does not affect existing disulfide bonds (Figure 3E), non-reducing SDS-PAGE (without DTT/β-mercaptoethanol to cleave disulfide bonds) and subsequent immunoblotting using anti-HMGB1 antibody detected a single HMGB1 band at the 29-kDa position without a 25-kDa band that correlates to the oxidized form of HMGB1 with an intramolecular Cys23–Cys45 disulfide bond in the medium of poly(I:C)- or SNP-treated RAW 264.7 cells (Figure 3F). Because both ROS and NO were produced after LPS challenge (Gao et al., 2002b; Tu et al., 2019), no significant influence of C23S or C45S mutation on LPS-triggered HA-HMGB1 secretion (Figures 4 and S2) indicated that oxidation or SNO of C23S or C45S was not essential for LPS-triggered HMGB1 secretion from macrophages. It has been reported that NO, at high levels, induces SNO of two vicinal cysteine thiols, thereby preventing them from forming a disulfide bond (Lipton et al., 2002; Uehara et al., 2006). During inflammation, iNOS-derived NO can reach a high level (micromolar ranges) and acts as a crucial inflammatory mediator (Kapil et al., 2020; Liu et al., 2002; MacMicking et al., 1997; Yeh et al., 2011). Thus, although it remained unclear whether Cys23 or Cys45 of secreted HMGB1 from inflammogen- or SNP-treated microglia/macrophages was in the free thiol or nitrosothiol conformation, the functional prevention of LPS- or SNP-elicited HA-HMGB1 secretion by C106S and C23SC45SC106S mutations, but not by C23S or C45S mutation, indicated that under inflammatory conditions, in which iNOS-derived NO reached high levels (micromolar ranges), SNO modification at Cys106 was essential and sufficient for inflammation-elicited HMGB1 secretion. Notably, the complete prevention of LPS-induced HMGB1 secretion from peripheral monocytes/macrophages into mouse serum and from brain microglia after an i.p. and intranigral LPS injection, respectively, by genetic deletion of iNOS (Figure 2), combined with the blockage of LPS- or poly(I:C)-elicited SNO and secretion of HMGB1 in cultured microglia/macrophages by iNOS inhibition (Figure 3), indicated that SNO modification of HMGB1 mediated by iNOS-derived NO was a preferential and key regulatory mechanism of HMGB1 secretion during inflammation.

This study demonstrated that posttranslational SNO modification of HMGB1 regulated its nucleocytoplasmic translocation and extracellular secretion in peripheral macrophages and brain microglia and identified a key cysteine residue (Cys106) for secretion-linked SNO. SNO-HMGB1 displayed stronger proinflammatory and neurodegenerative effects

than unmodified HMGB1. Mechanistically, SNO-HMGB1 bound to microglial Mac1 with higher affinity than unmodified HMGB1 and also bound to other HMGB1 receptors at high concentrations. The *in vivo* findings that HMGB1 injection induced chronic microglial activation, dopaminergic neurodegeneration, and locomotor deficit in WT mice but not $Mac1^{-/-}$ mice reinforced pathogenic roles of interaction of extracellular HMGB1 with microglial Mac1 receptor in PD development. Collectively, this study uncovered regulatory mechanisms of SNO modification on HMGB1 secretion and identified a mechanistic basis for inflammatory neurodegeneration and related locomotor impairment in PD. This study also suggests a therapeutic potential of HMGB1-targeting intervention for PD.

Limitations of the study

Our genetic, biochemical, and double-label immunofluorescence studies demonstrated that the posttranslational SNO modification at Cys106 was essential and sufficient for inflammation-elicited HMGB1 secretion. However, a limitation of our study is that we were not able to directly examine secreted WT HA-HMGB1 with SNO modification at Cys106 in the supernatant of LPS-treated primary macrophage cultures using liquid chromatography-mass spectrometry (LC-MS). In addition, our study revealed that LPS- or SNP-elicited nucleocytoplasmic shuttling and extracellular secretion of WT HA-HMGB1 were prevented by C106S and C23SC45SC106S mutations but not by C23S or C45S mutation. Additional site-specific identification of SNO modification of HA-HMGB1 using LC-MS can show whether Cys23 or Cys45 of secreted HMGB1 is in the free thiol or nitrosothiol conformation, thereby determining whether Cys23 and Cys45 are insensitive to SNO modification or SNO at Cys23 and/or Cys45 does not regulate HMGB1 secretion.

STAR METHODS

RESOURCE AVAILABILITY

Lead contact—Further information and requests for resources and reagents should be directed to and will be fulfilled by the lead contact, Hui-Ming Gao (gaohm@nju.edu.cn).

Materials availability—All plasmids generated in this study are available from the lead contact without restriction.

Data and code availability

- Original full immunoblot images have been deposited at Mendeley data and are publicly available as of the date of publication. The DOI (Mendeley Data: https://dx.doi:10.17632/zxs62xh37z.1) is also listed in the key resources table. Microscopy data reported in this paper will be shared by the lead contact upon request.
- This study does not generate or utilize any computer codes or algorithms.
- Any additional information required to reanalyze the data reported in this paper is available from the lead contact upon request.

EXPERIMENTAL MODEL AND SUBJECT DETAILS

Mice—Mice were maintained and bred in the standard cages under a condition of 12 h light-dark cycle in the specific-pathogen-free (SPF) animal facility credited by Association for Assessment and Accreditation of Laboratory Animal Care (AAALAC). B6.129P2–NOS2tm1Lau/J (iNOS$^{-/-}$ or NOS2$^{-/-}$) mice and wildtype (WT) control mice (C57BL/6J) were purchased from the Jackson Laboratory (Bar Harbor, ME) and used for the intranigral/i.p. injection of LPS at the NIEHS (Research Triangle Park, North Carolina, USA) following the National Institutes of Health Guide for Humane Care and Use of Laboratory Animals (Institute of Laboratory Animal Resources, 1996). B6.129S4–Itgamtm1Myd/J (Mac1$^{-/-}$) and B6.129S6–Cybbtm1Din/J (gp91$^{-/-}$, NADPH oxidase-deficient) mice were purchased from the Jackson Laboratory (Bar Harbor, ME). Breeding of C57BL/6, Mac1$^{-/-}$ and gp91$^{-/-}$ mice, preparation of various primary cell cultures using embryos, pups or adult mice, and intranigral injection of HMGB1 in Mac1$^{-/-}$ and C57BL/6 mice were conducted at the Model Animal Research Center of Nanjing University in accordance with the Guide for the Care and Use of Laboratory Animals of Nanjing University, Nanjing, China. All procedures were approved by Nanjing University or NIEHS Animal Care and Use Committee. Two-month-old mice were used for stereotaxic brain injection and preparation of peritoneal macrophages. Mouse embryos at gestation day 14 ± 0.5 or 1-day-old mouse pups were used for preparing primary cell cultures. Both male and female mice were used unbiasedly in all the animal experiments. The detailed information was described in the Method details section and the figure legends. All the animals were treated humanely. All efforts were made to minimize the number of animals and their suffering.

Cell cultures

Primary microglia-enriched cultures and BV2 microglial cell line: Primary microglia-enriched cultures were prepared from the whole brains of 1-day-old mouse pups as previously reported (Gao et al., 2002a). Briefly, mouse brain tissues, devoid of blood vessels and meninges, were dissociated by mild mechanical trituration. Disassociated brain cells (2.5×10^7 cells) were seeded in Corning® 100 mm TC-treated culture dishes in DMEM/F12 culture medium containing 10% heat-inactivated fetal bovine serum (FBS), 2 mM L-glutamine, 1 mM sodium pyruvate, 0.1 mM nonessential amino acids, 50 U/mL penicillin, and 50 μg/mL streptomycin. The medium was changed 4 days after seeding. On reaching confluence (12-14 days), microglia were separated from astrocytes by shaking the culture dish for 20 min at 150 rpm. Enriched microglia were collected by centrifugation, re-suspended in DMEM containing 10% FBS and 1 mM sodium pyruvate and plated into 24-(1×10^5/well), 12-(2×10^5/well) or 6-well (4×10^5/well) plates, Lab-Tek II chamber slides (Nalge Nunc, Rochester, NY) or glass-bottom microwell dishes (1×10^5/well). The enriched microglia cultures contained <1% glial fibrillary acidic protein (GFAP)-IR astroglia and >99% Iba1-IR microglia as determined by Immunocytochemistry. These enriched microglia prepared by mechanical dissociation and separation preserved the integrity and the relative quiescent state; their purity (>99%) basically excluded influence of astroglial contamination. BV2 mouse microglial cell line was maintained in high glucose DMEM supplemented with 10% heat-inactivated FBS, 50 U/mL penicillin, and 50 μg/mL streptomycin (Gao et al., 2003).

Peritoneal resident macrophages and raw 264.7 cells: Mature quiescent peritoneal macrophages were harvested from the peritoneal cavity of C57BL/6 mice by lavage in 5 mL of ice-cold RPMI medium 1640 (Thermo Fisher Scientific), washed twice, and pre-incubated in serum-free RPMI 1640 medium for 1 h. After non-adherent cells were removed by washing twice, adherent macrophages were transfected with plasmids immediately or cultured overnight in RPMI 1640 medium containing 10% heat-inactivated FBS before treatments. RAW 264.7 cells (the murine macrophage cell line) were maintained in DMEM (low glucose) containing 10% heat-inactivated FBS, 2 mM L-glutamine, 50 U/mL penicillin, and 50 μg/mL streptomycin (Zhou et al., 2013).

Primary midbrain neuron-glia cultures: Midbrain neuron-glia cultures were prepared from the ventral mesencephalon of C57BL/6 and Mac1$^{-/-}$ embryos at gestation day 14 ± 0.5 (Gao et al., 2002a). Dissociated midbrain cells with a gentle mechanical trituration were seeded into 24-well plates (6×10^5 cells/well) pre-coated overnight with poly-D-lysine (20 μg/mL). Cultures were maintained in MEM culture medium supplemented with 10% heat-inactivated FBS and horse serum (HS), 1 g/L glucose, 2 mM L-glutamine, 1 mM sodium pyruvate, and 0.1 mM nonessential amino acids. Seven days after seeding, cultures were treated with vehicle or desired reagents in MEM treatment medium containing 2% FBS, 2% HS, 2 mM L-glutamine, and 1 mM sodium pyruvate. At the time of treatment, the neuron-glia cultures were made up of ~10% microglia, 50% astrocytes, and 40% neurons of which 2.5-3.5% were TH-IR dopamine neurons (Gao et al., 2002a).

METHOD DETAILS

Stereotaxic injection into the substantia nigra (SN)—After the mice were anaesthetized with ketamine/xylazine (90 and 10 mg/kg respectively, i.p. injection), the intranigral injection of the desired reagents was performed over a period of 5 min (0.4 μL/min) under the control of a motorized microinjection pump as previously described (Gao et al., 2008). Briefly, sterile normal saline (2 μL) or LPS (Escherichia coli 0111:B4; Sigma-Aldrich; Cat# L3012; 3 μg in 2 μL of sterile saline) was stereotaxically injected into the left and the right side of the SN of iNOS$^{-/-}$ and WT mice respectively. The left and the right side of the SN of Mac1$^{-/-}$ and WT mice were injected with sterile normal saline (2 μL) and endotoxin-free recombinant HMGB1 protein (2 μg in 2 μL of sterile saline) respectively. As a control, saline and fatty acid-free BSA (2 μg) were injected into the left and the right side of the SN respectively. The following coordinates were used for the injection: 3.0 mm posterior to the bregma, 1.3 mm lateral to the midline, and 4.7 mm ventral to the surface of the skull. At 24 h after LPS injection or 1 month after HMGB1/BSA injection, mice were euthanized with fatal plus and then transcardially perfused with ice-cold PBS followed by PBS-buffered 4% paraformaldehyde. The brains were removed, post-fixed for 2 days at 4°C in 4% paraformaldehyde, and cryoprotected for 2-3 days at 4°C in PBS-buffered 30% sucrose. Coronal sections (30 μm in thickness) were cut with a microtome through the SN.

Chemical treatment—Unless otherwise indicated, various microglia/macrophages cultures were treated with vehicle, widely used inflammogen LPS (15 ng/mL; E. coli O111: B4; Calbiochem; Cat# 437,627) or poly (I:C) (a synthetic dsRNA and Toll-like receptor 3 agonist; 50 μg/mL; Sigma-Aldrich; Cat# P0913) or NO donor SNP (20 mM; Sigma-Aldrich;

Cat# 71778) or GSNO (50 μM; Sigma-Aldrich; Cat# N4148) for 24 h with or without pretreatment for 30 min with 10 μM 1400W (Sigma-Aldrich; Cat# W4262). Being light sensitive, NO donors and protein samples containing nitrosothiols were handled with light protection.

Confocal double-label immunofluorescence—Paraformaldehyde-fixed mouse brain sections and primary microglial cultures grown in glass-bottom microwell dishes (MatTek Corp, MA) or Lab-Tek II chamber slides (Nalge Nunc, Rochester, NY) were immunostained using rabbit polyclonal HMGB1 antibody (1:2000; ChIP Grade; Abcam; Cat# ab18256; RRID:AB_444360), in combination with rat polyclonal CD11b antibody (1:500; Bio-Rad Laboratories; Cat# MCA711G; RRID:AB_323167) or mouse monoclonal S-nitroso-cysteine (SNO-C) antibody (1:1000; Abcam; Cat# ab94930; RRID:AB_10697568). Peritoneal macrophages were immunostained with mouse monoclonal anti-GFP antibody (1:200; Beyotime) and rabbit monoclonal anti-HA antibody (1:1000; Cell Signaling Technology; Cat# 3724; RRID:AB_1549585). Brain sections and cell cultures were then incubated with the corresponding secondary antibodies conjugated with Alexa Fluor 488 and/or Alexa Fluor 594 (1:1000; Thermo Fisher Scientific; Cat# A-11029; RRID:AB_2534088; Cat# A-11034; RRID:AB_2576217; Cat# A-11032; RRID:AB_2534091; Cat# A-11037; RRID:AB_2534095) followed by nuclear counterstaining using DAPI (4’,6-diamidino-2-phenylindole). Fluorescent images were obtained with a Zeiss LSM880 Laser Scanning Confocal Microscope (Carl Zeiss Microimaging Inc.) and analyzed by using ImageJ software. Notably, the single projection and the maximum intensity projection of a Z-stack of 30 confocal fluorescent images from a brain slice taken at 1 μm step size (Figures 1A and 2C) not only displayed 3D structure of microglia in 2D images with greater clarity and more details but also better presented membrane staining of CD11b and nuclear staining of HMGB1.

Immunocytochemistry and cell count—Paraformaldehyde-fixed mouse brain sections and neuron-glia cultures were immunostained following our published protocols (Gao et al., 2002a). Briefly, cell cultures were blocked with appropriate normal serum followed by incubation overnight at 4°C with primary antibodies against TH for dopamine neurons (1:5000; Millipore; Cat# AB152; RRID:AB_390204); Iba1 (1:1500; Wako; Cat# 019-19741; RRID:AB_839504) and CD11b (1:500; Bio-Rad Laboratories; Cat# MCA711G; RRID:AB_323167) for microglia/macrophages, TMEM119 (1:500; Synaptic Systems; Cat# 400,011; RRID:AB_2782984) for brain microglia; Neu-N (1:2000; Sigma/Merck/Millipore; Cat# MAB377; RRID:AB_2298772) and MAP-2 (1:400; Millipore; Cat# MAB3418; RRID:AB_94856) for neurons, or GFAP (1:1000; Agilent; Cat# Z0334; RRID:AB_10013382) for astroglia. After incubation with an appropriate biotinylated secondary antibody and then the Vectastain ABC reagents (Vector Laboratory; Cat# PK-6100), the bound complex was visualized by color development with 3,3’-diaminobenzidine (DAB). Following immunostaining, numbers of TH-IR dopamine neurons in the SN as well as numbers of Neu-N-IR neurons and Iba1-IR microglia in the culture were counted by two investigators in a blind manner. The optical density of Iba1 or MAP-2 immunoreactivity in the SN or the cell culture was measured from images taken from the SN region or each well (ten images) of culture plates and analyzed by using ImageJ software.

Eight and four evenly spaced brain sections from a series of 24 sections that covered the entire SN were used for the count of TH-IR neurons and the measurement of the optical density of Iba1 immunoreactivity in nigral microglia respectively by two individuals blind to the treatment. For each *in vitro* experiment, 2–3 wells/treatment condition were used for cell counting and optical density measurement. Results from three to five independent experiments were obtained and analyzed, as described in the corresponding figure legend.

Nuclear fractionation—Nuclear proteins were extracted from BV2 microglial cells at 4°C using buffers containing 1 mM PMSF and 1:100 protease inhibitor cocktail (Gao et al., 2011b). After centrifugation at 2000 × g for 10 min, cells pellets were fully suspended with vigorous vortex at the highest speed in buffer A (10 mM HEPES at PH 8.0, 1.5 mM $MgCl_2$, 10 mM KCl, and 1mM dithiothreitol) and incubated on ice for 15 min with frequent vortex and pipetting/passing through a 25-gauge needle 10 times. The lysis completion was monitored by trypan blue staining. The lysate was centrifuged at 3000 × g for 15 min. The recovered nuclear pellets were washed twice with vigorous vortex for 15 s for suspension and incubated on ice for 40 min with continuous vortexing for 15 s every 10 min with buffer B (60 mM NaCl, 10 mM HEPES at pH 8.0, 25% glycerol, 0.1 mM EDTA, and 1 mM dithiothreitol). Washed nuclei were extracted with buffer C (20 mM HEPES at pH 7.5, 25% glycerol, 420 mM NaCl, 1.5 mM $MgCl_2$, 0.2 mM EDTA, and 1 mM dithiothreitol). The nuclear suspension was centrifuged at 13,000 × g for 30 min, and the supernatant was collected as a nuclear fraction.

Gel electrophoresis and immunoblotting analysis—Proteins were extracted from cultured cells using RIPA lysis buffer (50 mM Tris-HCl, pH 8.0, 150 mM NaCl, 5 mM EDTA, 1% nonidet P-40, 0.5% sodium deoxycholate, 0.1% sodium dodecyl sulfate [SDS], and 1:100 protease inhibitor cocktail). The culture medium collected from treated microglia or macrophage cultures was concentrated before electrophoresis with Amicon Ultra-4 Centrifugal filter units (10,000 NMWL; Cat# UFC801024; Millipore) at 4°C. Protein denaturation was performed by heated to 95°C for 10 min. Protein samples were resolved on 12% SDS-PAGE gels, and Immunoblotting analyses were performed using antibodies against Iba1 (1:3000; Wako Pure Chemicals), iNOS (1:1000; Cell Signaling Technology; Cat# 13120; RRID:AB_2687529), HMGB1 (1:4000; Abcam), SNO-C (1:1000; Abcam), biotin (1:1000; Santa Cruz Technology; Cat# sc-101339; RRID:AB_1119609), TH (1:5000; Millipore), PSD95 (postsynaptic density protein 95; 1:2000; Millipore; Cat# MABN68; RRID:AB_10807979), Neu-N (1:1000; Sigma/Merck/Millipore) or GFAP (1:1000, Santa Cruz Biotechnology; Cat# sc-65343; RRID:AB_783553). An antibody against β-actin (1:5000; Cell Signaling Technology; Cat#8457; RRID:AB_10950489), GAPDH (1:5000; Cell Signaling Technology; Cat# 2118; RRID: AB_561053), or histone H3 (an internal control of the nuclear protein; 1:1000, Bioworld; Cat# BS1174; RRID:AB_1663967) was included as an internal standard to monitor loading errors. Note: The representative immunoblotting and immunostaining images were presented, and the repeat number of *in vitro* experiments or the mouse number in one (Figures 1A and 7A) or two independent (Figures 2A and 2C) *in vivo* experiment(s) was indicated in the corresponding quantification data in each corresponding figure.

Immunoprecipitation—The Immunoprecipitation experiment was performed as described before (Gao et al., 2011b). The culture medium, collected from BV2 cells treated with vehicle, poly (I:C) or SNP for 24 h, was concentrated with Amicon Ultra-4 Centrifugal filter units and then successively incubated with anti-HMGB1 antibody (2 μg; Abcam) overnight and protein A-Sepharose slurry for 2 h at 4°C. Protein A beads were collected by centrifugation at 2000 × g for 5 min and washed six times with TNE buffer (10 mM Tris-HCl at pH 7.5, 1% nonidet P-40, 150 mM NaCl, 1 mM EDTA, and 1:100 protease inhibitor cocktail). Bound proteins were eluted in sample buffer, separated on 12% SDS-PAGE gels, blotted with anti-SNO-C antibody first and then re-probed for HMGB1 after stripping the membrane.

Nitrite assay—The production of NO was determined by measuring the level of nitrite (the stable end-product of NO and a widely used parameter for measurement of NO production) in the culture medium with the Griess reagent (1% sulfanilamide, 2.5% phosphoric acid, 0.1% N-1-napthylethylenediamine dihydrochloride). The absorbance at wavelength 540 nm was measured.

MTT cytotoxicity assay—To exclude the possibility of HMGB1 release by necrotic cells resulting from non-specific cytotoxicity, microglia-enriched cultures were treated for 24 h with various reagents as specified in the figure legend and then incubated with 1 mg/mL MTT (Sigma-Aldrich) for 90 min at 37°C. Precipitated formazan crystals, products of MTT tetrazolium ring by the action of mitochondrial dehydrogenases, were solubilized with DMSO and quantified spectrophotometrically at 570 nm.

Biotin-switch assay—Biotin-switch assay, a method to specifically detect S-nitrosylated proteins, was performed as described (Jaffrey and Snyder, 2001), with minor modifications. Briefly, supernatant proteins from Raw 264.7 cells or peritoneal macrophages treated with desired reagents were adjusted to 0.8 mg/mL with HENS buffer (250 mM HEPES, pH 7.7, 1 mM EDTA, 0.1 mM neocuproine and 1% SDS). To block free thiols of cysteine residues, protein samples were incubated at 50°C for 20 min with 4 volumes of the blocking buffer, which is the HENS buffer supplemented with 2.5% SDS and 20 mM MMTS (a thiol-specific methylthiolating reagent). After removal of unreacted MMTS by acetone precipitation and centrifugation, the protein pellet was re-suspended in HENS buffer and then adjusted to contain 4 mM ascorbate and 4 mM biotin–HPDP (a sulfhydryl-specific biotinylating agent). During incubation for 1 h at 25°C, cysteines' S-nitrosothiols of the blocked protein samples were reduced to free thiols by ascorbate, and the newly formed free thiols (i.e., initial S-nitrosothiols) were immediately biotinylated by biotin–HPDP. Because the biotin-switch reaction does not affect existing disulfide bonds (Figure 3E), non-reducing SDS-PAGE (without DTT/β-mercaptoethanol to cleave disulfide bonds) and following immunoblotting using anti-HMGB1 and anti-biotin antibodies were utilized to examine possible co-existence and cross-regulation between oxidation and SNO on HMGB1. Non-reducing sample buffer (50 mM Tris-HCl, pH 6.8, 30% glycerol, 10% SDS, and 0.01% bromophenol blue) was added to biotinylated proteins that were immediately loaded onto the SDS-PAGE gel without boiling or reducing agent. Note: Before Immunoblotting to detect biotinylated proteins using anti-biotin mouse monoclonal antibody (1:1000; Santa Cruz, sc-101339), the TBS buffer

containing 5% BSA but not milk products was used to block unoccupied surfaces of the PVDF transfer membranes.

Plasmid vector construction and transfection—The recombinant pCS2(+)-4HA-HMGB1 plasmid vector was made by inserting the reverse transcription (RT)-PCR-generated HMGB1 coding sequence into the EcoRI and BglII sites of pCS2(+)-4HA (a gift from Dr. Zhen Zhu from Nanjing University) to produce a HA-HMGB1 fusion gene by homologous recombination. Using the primers 5'-ggagaaacttcagaccggacg-3' (F) and 5'-gggctatctaaagacacattcgg-3' (R), a genomic fragment of the HMGB1 gene was amplified by PCR using murine genomic DNA as a template. The primers 5'-tacgctggccggcctgaattcggcaaaggagatcctaaaaagccga-3' (F) and 5'-gctatctagtcatgaagatctctgcgctagaaccaacttattcatc-3' (R) were used to introduce homologous sequences of linearized pCS2(+)-4HA vector ends (21 bp containing EcoRI/BglII cutting site) into the 5'-end of the inserts by PCR amplification.

Site-directed mutagenesis was performed using the Mut Express® II Fast Mutagenesis Kit V2 (Vazyme, Cat# C214) following the manufacturer's instructions using appropriate PCR primer pairs that contained the desired mutation: 5'-gtgcaaacctcgagggaggagcacaagaagaagcac-3' (F1) and 5'- ctcctccctcgaggtttgcacaaagaatgcatatgaggacat-3' (R1) for the C23S-XhoI mutant; 5'-tccaagaagtcctcagagaggtggaagaccatgtctg-3' (F2) and 5'- cctctctgaggacttcttggagaactctgagaagttgacag-3' (R2) for the C45S mutant; 5'- ttcttgttctcttctgagtaccgccccaaaatcaaag-3' (F3) and 5'-gtactcagaagagaacaagaagaaggccgaaggagg-3' (R3) for C106S mutant. The triple mutant C23SC45SC106S were obtained by sequential rounds of mutagenesis. All constructs used in this study were verified by extensive restriction digestion and DNA sequencing.

Plasmid transfection in peritoneal macrophages—At 1 h after plating the cells from peritoneal lavage and immediately after removing non-adherent cells by washing the cultures twice, the freshly prepared peritoneal resident macrophages were transfected with plasmids pCS2(+)-4HA-HMGB1 and pLVX-GFP following the manufacturer's instructions and a previous publication (Kong et al., 2016) with modifications. To avoid possible influence of remarkably increased protein size on HMGB1 secretion, we did not construct GFP-HMGB1-expressing plasmid. Among several transfection reagents we screened, the LipoMax transfection reagent (SUDGEN, Cat# 32010) exhibited the highest transfection efficiency and the least cytotoxicity during the plasmid transfection in primary macrophages. In order to avoid possible influence of overexpression of too much HA-HMGB1 on the physiological location and the secretion mechanism of endogenous HMGB1 and HA-HMGB1, we adjusted the amount of plasmids (0.3 μg each plasmid per chamber/24-well) and the transfection duration to achieve "a low level" of HA-HMGB1 expression in macrophages. The plasmid DNA-LipoMax complex was prepared in antibiotic-free Opti-MEM® I reduced serum medium following the manufacturer's instructions and was added (with 1:10 dilution) to RPMI-1640 medium containing 10% FBS. After plasmid transfection for 48 h in this medium, the cultures were then changed to normal treatment medium (RPMI-1640 medium containing 2% FBS) and treated with vehicle, LPSorSNP. At 24

h after the treatment, nucleocytoplasmic translocation and secretion of HA-HMGB1 was examined by confocal double-label immunofluorescence. We quantified HA fluorescent intensity in macrophages co-transfected with the two plasmids. This method better discriminated the cells whose cytosolic HA staining was weak and nuclear HA-HMGB1 was "emptied" after LPS/SNP treatment from non-transfected cells. As expected, GFP expression did not affect the subcellular location of various HA-HMGB1.

***In vitro* SNO—**To prevent light-induced degradation of NO donors or protein nitrosothiols, all reagents/samples were protected from light by covering tubes and containers with foil during *in vitro* SNO reaction. Endotoxin-free recombinant HMGB1 protein (2.5 μg/mL in sterile normal saline; Biolegend; Cat# 764,006) or saline was incubated with NO donor GSNO (50 μM) or saline in the dark for 1 h at 37°C. Then 50 μL of the reaction mixture was added to midbrain neuron-glia cultures containing 450 μL of the treatment medium. Thus, after possible decomposition of GSNO during 1-h *in vitro* incubation at 37°C, the medium contained less than 5 μM GSNO with or without 250 ng/mL SNO-HMGB1. The four treatment groups were called "Saline", "HMGB1"that contained unmodified HMGB1, "incubated GSNO" or "SNO-HMGB1". At 7 days after the treatment, neurodegeneration was evaluated by Immunocytochemistry, cell count and Immunoblotting.

Rotarod behavior test—The rotarod behavior test was performed on ZB-200 Rota-Rod Instrument (TECHMAN Technology Co). The start speed, the acceleration rate, and the maximum speed were set to 1 rpm, 0.5 rpm/10s, and 50 rpm, respectively. The mice underwent three trials with 30-min interval per day for two consecutive days. The latency time to fall from the rotating rod was recorded and analyzed to evaluate the motor coordination and balance of mice. Before and between test trials, the Instrument was cleaned thoroughly with 70% ethanol and ddH_2O.

Open field test—The open field test examines exploratory behaviors and anxiety-related behaviors. Prior to the open field test, the mice were habituated to the behavioral testing room for 30 min. During the test, the mouse was allowed to freely explore a square open field apparatus (40.5 cm × 40.5 cm × 35.5 cm) for 20 min. Before and between tests, the apparatus was cleaned thoroughly with 70% ethanol and ddH_2O. All activities of each mouse were tracked via a camera linked to a computer monitoring system. Time spent and distance traveled in the central zone (27 cm × 27 cm area in the center of the open field apparatus) and the peripheral zone were analyzed by the software TopScan Lite (Clever Sys Inc.).

QUANTIFICATION AND STATISTICAL ANALYSIS

All data were analyzed using GraphPad Prism 7 software. All values are expressed as the mean ± SEM from combined data from multiple independent *in vitro* experiments or from multiple independent mice in one (Figures 1B and 7B–D) or two independent (Figures 2B and 2D) *in vivo* experiment(s). The repeat number of *in vitro* experiments (n) and the mouse number (n) from the two repeated *in vivo* experiments were shown in the corresponding figure legend. Differences among means were analyzed by using unpaired two-sample t tests and one- or two-way ANOVA with treatment or genotype as the independent factors. When

ANOVA showed significant differences, multiple comparisons between means were tested by Dunnett's, Tukey's, or Sidak's multiple post hoc testing, as described in detail in the corresponding figure legends. In all analyses, the null hypothesis was rejected at the 0.05 level.

Supplementary Material

Refer to Web version on PubMed Central for supplementary material.

ACKNOWLEDGMENTS

This work was supported by the National Natural Science Foundation of China (grant 31471006), the National High Technology Research and Development Program of China (grant 2014AA021601), the Fundamental Research Funds of Central University (021414380524), the Priority Academic Program Development of Jiangsu Higher Education Institutions, and the Award to High-Level Innovative and Entrepreneurial Talents of Jiangsu Province of China (0903/133032) to H.-M.G. This work was supported in part by the Intramural Research Program of the NIH/NIEHS in the United States (ES090082) to J.-S.H.

REFERENCES

Abu-Soud HM, Gachhui R, Raushel FM, and Stuehr DJ (1997). The ferrous-dioxy complex of neuronal nitric oxide synthase. Divergent effects of L-arginine and tetrahydrobiopterin on its stability. J. Biol. Chem 272, 17349–17353. 10.1074/jbc.272.28.17349. [PubMed: 9211873]

Andrassy M, Volz HC, Igwe JC, Funke B, Eichberger SN, Kaya Z, Buss S, Autschbach F, Pleger ST, Lukic IK, et al. (2008). High-mobility group box-1 in ischemia-reperfusion injury of the heart. Circulation 117, 3216–3226. 10.1161/CIRCULATIONAHA.108.769331. [PubMed: 18574060]

Benedet PO, Menegatti ACO, Gonçalves MC, Terenzi H, and Assreuy J (2018). The therapeutic value of protein (de)nitrosylation in experimental septic shock. Biochim. Biophys. Acta, Mol. Basis Dis 1864, 307–316. 10.1016/j.bbadis.2017.10.029. [PubMed: 29111468]

Bonaldi T, Talamo F, Scaffidi P, Ferrera D, Porto A, Bachi A, Rubartelli A, Agresti A, and Bianchi ME (2003). Monocytic cells hyperacetylate chromatin protein HMGB1 to redirect it towards secretion. EMBO J. 22, 5551–5560. 10.1093/emboj/cdg516. [PubMed: 14532127]

Choi MS, Nakamura T, Cho SJ, Han X, Holland EA, Qu J, Petsko GA, Yates JR 3rd, Liddington RC, and Lipton SA (2014). Transnitrosylation from DJ-1 to PTEN attenuates neuronal cell death in Parkinson's disease models. J. Neurosci 34, 15123–15131. 10.1523/JNEUROSCI.4751-13.2014. [PubMed: 25378175]

Deng M, Tang Y, Li W, Wang X, Zhang R, Zhang X, Zhao X, Liu J, Tang C, Liu Z, et al. (2018). The endotoxin delivery protein HMGB1 mediates caspase-11-dependent lethality in sepsis. Immunity 49, 740–753.e7. 10.1016/j.immuni.2018.08.016. [PubMed: 30314759]

Elenkov I, Pelovsky P, Ugrinova I, Takahashi M, and Pasheva E (2011). The DNA binding and bending activities of truncated tail-less HMGB1 protein are differentially affected by Lys-2 and Lys-81 residues and their acetylation. Int. J. Biol. Sci 7, 691–699. 10.7150/ijbs.7.691. [PubMed: 21647302]

Fauconnier J, Meli AC, Thireau J, Roberge S, Shan J, Sassi Y, Reiken SR, Rauzier JM, Marchand A, Chauvier D, et al. (2011). Ryanodine receptor leak mediated by caspase-8 activation leads to left ventricular injury after myocardial ischemia-reperfusion. Proc. Natl. Acad. Sci. USA 108, 13258–13263. 10.1073/pnas.1100286108. [PubMed: 21788490]

Foster MW, Hess DT, and Stamler JS (2009). Protein S-nitrosylation in health and disease: a current perspective. Trends Mol. Med 15, 391–404. 10.1016/j.molmed.2009.06.007. [PubMed: 19726230]

Gadani SP, Walsh JT, Lukens JR, and Kipnis J (2015). Dealing with danger in the CNS: the response of the immune system to injury. Neuron 87, 47–62. 10.1016/j.neuron.2015.05.019. [PubMed: 26139369]

Gaikwad S, Puangmalai N, Bittar A, Montalbano M, Garcia S, McAllen S, Bhatt N, Sonawane M, Sengupta U, and Kayed R (2021). Tau oligomer induced HMGB1 release contributes to cellular

senescence and neuropathology linked to Alzheimer's disease and frontotemporal dementia. Cell Rep. 36, 109419. 10.1016/j.celrep.2021.109419. [PubMed: 34289368]

Gao HM, Hong JS, Zhang W, and Liu B (2002a). Distinct role for microglia in rotenone-induced degeneration of dopaminergic neurons. J. Neurosci 22, 782–790. [PubMed: 11826108]

Gao HM, Jiang J, Wilson B, Zhang W, Hong JS, and Liu B (2002b). Microglial activation-mediated delayed and progressive degeneration of rat nigral dopaminergic neurons: relevance to Parkinson's disease. J. Neurochem 81, 1285–1297. 10.1046/j.1471-4159.2002.00928.x. [PubMed: 12068076]

Gao HM, Kotzbauer PT, Uryu K, Leight S, Trojanowski JQ, and Lee VMY (2008). Neuroinflammation and oxidation/nitration of α-synuclein linked to dopaminergic neurodegeneration. J. Neurosci 28, 7687–7698. 10.1523/JNEUROSCI.0143-07.2008. [PubMed: 18650345]

Gao HM, Liu B, Zhang W, and Hong JS (2003). Critical role of microglial NADPH oxidase-derived free radicals in the in vitro MPTP model of Parkinson's disease. FASEB J 17, 1954–1956. 10.1096/fj.03-0109fje.t. [PubMed: 12897068]

Gao HM, Zhang F, Zhou H, Kam W, Wilson B, and Hong JS (2011a). Neuroinflammation and α-synuclein dysfunction potentiate each other, driving chronic progression of neurodegeneration in a mouse model of Parkinson's disease. Environ. Health Perspect 119, 807–814. 10.1289/ehp.1003013. [PubMed: 21245015]

Gao HM, Zhou H, and Hong JS (2012). NADPH oxidases: novel therapeutic targets for neurodegenerative diseases. Trends Pharmacol. Sci 33, 295–303. 10.1016/j.tips.2012.03.008. [PubMed: 22503440]

Gao HM, Zhou H, Zhang F, Wilson BC, Kam W, and Hong JS (2011b). HMGB1 acts on microglia Mac1 to mediate chronic neuroinflammation that drives progressive neurodegeneration. J. Neurosci 31, 1081–1092. 10.1523/JNEUROSCI.3732-10.2011. [PubMed: 21248133]

Garbán HJ, Márquez-Garbán DC, Pietras RJ, and Ignarro LJ (2005). Rapid nitric oxide-mediated S-nitrosylation of estrogen receptor: regulation of estrogen-dependent gene transcription. Proc. Natl. Acad. Sci. USA 102, 2632–2636. 10.1073/pnas.0409854102. [PubMed: 15699347]

Gardella S, Andrei C, Ferrera D, Lotti LV, Torrisi MR, Bianchi ME, and Rubartelli A (2002). The nuclear protein HMGB1 is secreted by monocytes via a non-classical, vesicle-mediated secretory pathway. EMBO Rep. 3, 995–1001. 10.1093/embo-reports/kvf198. [PubMed: 12231511]

Gdynia G, Sauer SW, Kopitz J, Fuchs D, Duglova K, Ruppert T, Miller M, Pahl J, Cerwenka A, Enders M, et al. (2016). The HMGB1 protein induces a metabolic type of tumour cell death by blocking aerobic respiration. Nat. Commun 7, 10764. 10.1038/ncomms10764. [PubMed: 26948869]

Gross TJ, Kremens K, Powers LS, Brink B, Knutson T, Domann FE, Philibert RA, Milhem MM, and Monick MM (2014). Epigenetic silencing of the human NOS2 gene: rethinking the role of nitric oxide in human macrophage inflammatory responses. J. Immunol 192, 2326–2338. 10.4049/jimmunol.1301758. [PubMed: 24477906]

Hara MR, Agrawal N, Kim SF, Cascio MB, Fujimuro M, Ozeki Y, Takahashi M, Cheah JH, Tankou SK, Hester LD, et al. (2005). S-nitrosylated GAPDH initiates apoptotic cell death by nuclear translocation following Siah1 binding. Nat. Cell Biol 7, 665–674. 10.1038/ncb1268. [PubMed: 15951807]

Haun F, Nakamura T, Shiu AD, Cho DH, Tsunemi T, Holland EA, La Spada AR, and Lipton SA (2013). S-nitrosylation of dynamin-related protein 1 mediates mutant huntingtin-induced mitochondrial fragmentation and neuronal injury in Huntington's disease. Antioxid. Redox Signal 19, 1173–1184. 10.1089/ars.2012.4928. [PubMed: 23641925]

Hess DT, Matsumoto A, Kim SO, Marshall HE, and Stamler JS (2005). Protein S-nitrosylation: purview and parameters. Nat. Rev. Mol. Cell Biol 6, 150–166. 10.1038/nrm1569. [PubMed: 15688001]

Hoppe G, Talcott KE, Bhattacharya SK, Crabb JW, and Sears JE (2006). Molecular basis for the redox control of nuclear transport of the structural chromatin protein Hmgb1. Exp. Cell Res 312, 3526–3538. 10.1016/j.yexcr.2006.07.020. [PubMed: 16962095]

Hotchkiss RS, and Karl IE (2003). The pathophysiology and treatment of sepsis. N. Engl. J. Med 348, 138–150. 10.1056/NEJMra021333. [PubMed: 12519925]

Jaffrey SR, and Snyder SH (2001). The biotin switch method for the detection of S-nitrosylated proteins. Sci. STKE 2001, pl1. 10.1126/stke.2001.86.pl1.

Kapil V, Khambata RS, Jones DA, Rathod K, Primus C, Massimo G, Fukuto JM, and Ahluwalia A (2020). The noncanonical pathway for *in vivo* nitric oxide generation: the nitrate-nitrite-nitric oxide pathway. Pharmacol. Rev 72, 692–766. 10.1124/pr.120.019240. [PubMed: 32576603]

Kone BC, Kuncewicz T, Zhang W, and Yu ZY (2003). Protein interactions with nitric oxide synthases: controlling the right time, the right place, and the right amount of nitric oxide. Am. J. Physiol. Renal Physiol 285, F178–F190. 10.1152/ajprenal.00048.2003. [PubMed: 12842859]

Kong D, Shen Y, Liu G, Zuo S, Ji Y, Lu A, Nakamura M, Lazarus M, Stratakis CA, Breyer RM, and Yu Y (2016). PKA regulatory IIα subunit is essential for PGD2-mediated resolution of inflammation. J. Exp. Med 213, 2209–2226. 10.1084/jem.20160459. [PubMed: 27621415]

Kwak MS, Kim HS, Lkhamsuren K, Kim YH, Han MG, Shin JM, Park IH, Rhee WJ, Lee SK, Rhee SG, and Shin JS (2019). Peroxiredoxin-mediated disulfide bond formation is required for nucleocytoplasmic translocation and secretion of HMGB1 in response to inflammatory stimuli. Redox Biol. 24, 101203. 10.1016/j.redox.2019.101203. [PubMed: 31026770]

Lipton SA, Choi YB, Takahashi H, Zhang D, Li W, Godzik A, and Bankston LA (2002). Cysteine regulation of protein function–as exemplified by NMDA-receptor modulation. Trends Neurosci. 25, 474–480. 10.1016/s0166-2236(02)02245-2. [PubMed: 12183209]

Liu B, Gao HM, Wang JY, Jeohn GH, Cooper CL, and Hong JS (2002). Role of nitric oxide in inflammation-mediated neurodegeneration. Ann. N. Y. Acad. Sci 962, 318–331. 10.1111/j.1749-6632.2002.tb04077.x. [PubMed: 12076984]

Lu B, Antoine DJ, Kwan K, Lundbäck P, Wähämaa H, Schierbeck H, Robinson M, Van Zoelen MAD, Yang H, Li J, et al. (2014). JAK/STAT1 signaling promotes HMGB1 hyperacetylation and nuclear translocation. Proc. Natl. Acad. Sci. USA 111, 3068–3073. 10.1073/pnas.1316925111. [PubMed: 24469805]

Lu B, Nakamura T, Inouye K, Li J, Tang Y, Lundbäck P, Valdes-Ferrer SI, Olofsson PS, Kalb T, Roth J, et al. (2012). Novel role of PKR in inflammasome activation and HMGB1 release. Nature 488, 670–674. 10.1038/nature11290. [PubMed: 22801494]

MacMicking J, Xie QW, and Nathan C (1997). Nitric oxide and macrophage function. Annu. Rev. Immunol 15, 323–350. 10.1146/annurev.immunol.15.1.323. [PubMed: 9143691]

Moldogazieva NT, Lutsenko SV, and Terentiev AA (2018). Reactive oxygen and nitrogen species-induced protein modifications: implication in carcinogenesis and anticancer therapy. Cancer Res. 78, 6040–6047. 10.1158/0008-5472.CAN-18-0980. [PubMed: 30327380]

Müller S, Ronfani L, and Bianchi ME (2004). Regulated expression and subcellular localization of HMGB1, a chromatin protein with a cytokine function. J. Intern. Med 255, 332–343. 10.1111/j.1365-2796.2003.01296.x. [PubMed: 14871457]

Nakamura T, and Lipton SA (2016). Protein S-nitrosylation as a therapeutic target for neurodegenerative diseases. Trends Pharmacol. Sci 37, 73–84. 10.1016/j.tips.2015.10.002. [PubMed: 26707925]

Nakamura T, Oh CK, Liao L, Zhang X, Lopez KM, Gibbs D, Deal AK, Scott HR, Spencer B, Masliah E, et al. (2021). Noncanonical transnitrosylation network contributes to synapse loss in Alzheimer's disease. Science 371, eaaw0843. 10.1126/science.aaw0843. [PubMed: 33273062]

Nakamura T, Tu S, Akhtar MW, Sunico CR, Okamoto SI, and Lipton SA (2013). Aberrant protein s-nitrosylation in neurodegenerative diseases. Neuron 78, 596–614. 10.1016/j.neuron.2013.05.005. [PubMed: 23719160]

Rizza S, Cardaci S, Montagna C, Di Giacomo G, De Zio D, Bordi M, Maiani E, Campello S, Borreca A, Puca AA, et al. (2018). S-nitrosylation drives cell senescence and aging in mammals by controlling mitochondrial dynamics and mitophagy. Proc. Natl. Acad. Sci. USA 115, E3388–E3397. 10.1073/pnas.1722452115. [PubMed: 29581312]

Seth D, Hess DT, Hausladen A, Wang L, Wang YJ, and Stamler JS (2018). A multiplex enzymatic machinery for cellular protein S-nitrosylation. Mol. Cell 69, 451–464.e6. 10.1016/j.molcel.2017.12.025. [PubMed: 29358078]

Sharma JN, Al-Omran A, and Parvathy SS (2007). Role of nitric oxide in inflammatory diseases. Inflammopharmacology 15, 252–259. 10.1007/s10787-007-0013-x. [PubMed: 18236016]

Sims GP, Rowe DC, Rietdijk ST, Herbst R, and Coyle AJ (2010). HMGB1 and RAGE in inflammation and cancer. Annu. Rev. Immunol 28, 367–388. 10.1146/annurev.immunol.021908.132603. [PubMed: 20192808]

Singh V, Roth S, Veltkamp R, and Liesz A (2016). HMGB1 as a key mediator of immune mechanisms in ischemic stroke. Antioxid. Redox Signal 24, 635–651. 10.1089/ars.2015.6397. [PubMed: 26493086]

Stamler JS, and Meissner G (2001). Physiology of nitric oxide in skeletal muscle. Physiol. Rev 81, 209–237. 10.1152/physrev.2001.81.1.209. [PubMed: 11152758]

Tang D, Kang R, Livesey KM, Cheh CW, Farkas A, Loughran P, Hoppe G, Bianchi ME, Tracey KJ, Zeh HJ 3rd, and Lotze MT (2010). Endogenous HMGB1 regulates autophagy. J. Cell Biol 190, 881–892. 10.1083/jcb.200911078. [PubMed: 20819940]

Tang D, Kang R, Livesey KM, Kroemer G, Billiar TR, Van Houten B, Zeh HJ 3rd, and Lotze MT (2011). High-mobility group box 1 is essential for mitochondrial quality control. Cell Metab. 13, 701–711. 10.1016/j.cmet.2011.04.008. [PubMed: 21641551]

Tu D, Gao Y, Yang R, Guan T, Hong JS, and Gao HM (2019). The pentose phosphate pathway regulates chronic neuroinflammation and dopaminergic neurodegeneration. J. Neuroinflammation 16, 255. 10.1186/s12974-019-1659-1. [PubMed: 31805953]

Uehara T, Nakamura T, Yao D, Shi ZQ, Gu Z, Ma Y, Masliah E, Nomura Y, and Lipton SA (2006). S-nitrosylated protein-disulphide isomerase links protein misfolding to neurodegeneration. Nature 441, 513–517. 10.1038/nature04782. [PubMed: 16724068]

Venereau E, Casalgrandi M, Schiraldi M, Antoine DJ, Cattaneo A, De Marchis F, Liu J,Antonelli A, Preti A, Raeli L, et al. (2012). Mutually exclusive redox forms of HMGB1 promote cell recruitment or proinflammatory cytokine release. J. Exp. Med 209, 1519–1528. 10.1084/jem.20120189. [PubMed: 22869893]

Wang H, Bloom O, Zhang M, Vishnubhakat JM, Ombrellino M, Che J, Frazier A, Yang H, Ivanova S, Borovikova L, et al. (1999). HMG-1 as a late mediator of endotoxin lethality in mice. Science 285, 248–251. 10.1126/science.285.5425.248. [PubMed: 10398600]

Yeh CH, Chou W, Chu CC, So EC, Chang HC, Wang JJ, and Hsing CH (2011). Anticancer agent 2-methoxyestradiol improves survival in septic mice by reducing the production of cytokines and nitric oxide. Shock 36, 510–516. 10.1097/SHK.0b013e318231866f. [PubMed: 21841536]

Youn JH, and Shin JS (2006). Nucleocytoplasmic shuttling of HMGB1 is regulated by phosphorylation that redirects it toward secretion. J. Immunol 177, 7889–7897. 10.4049/jimmunol.177.11.7889. [PubMed: 17114460]

Zhou H, Liao J,Aloor J, Nie H, Wilson BC, Fessler MB, Gao HM, and Hong JS (2013). CD11b/CD18 (Mac-1) is a novel surface receptor for extracellular double-stranded RNA to mediate cellular inflammatory responses. J. Immunol 190, 115–125. 10.4049/jimmunol.1202136. [PubMed: 23209319]

Highlights

- S-nitrosylation (SNO) by iNOS-derived nitric oxide (NO) regulates HMGB1 secretion
- SNO at Cys106 is essential and sufficient for inflammation-elicited HMGB1 secretion
- SNO of HMGB1 promotes its proinflammatory and neurodegenerative effects
- HMGB1-Mac1 interaction induces inflammation, neurodegeneration, and locomotor deficit

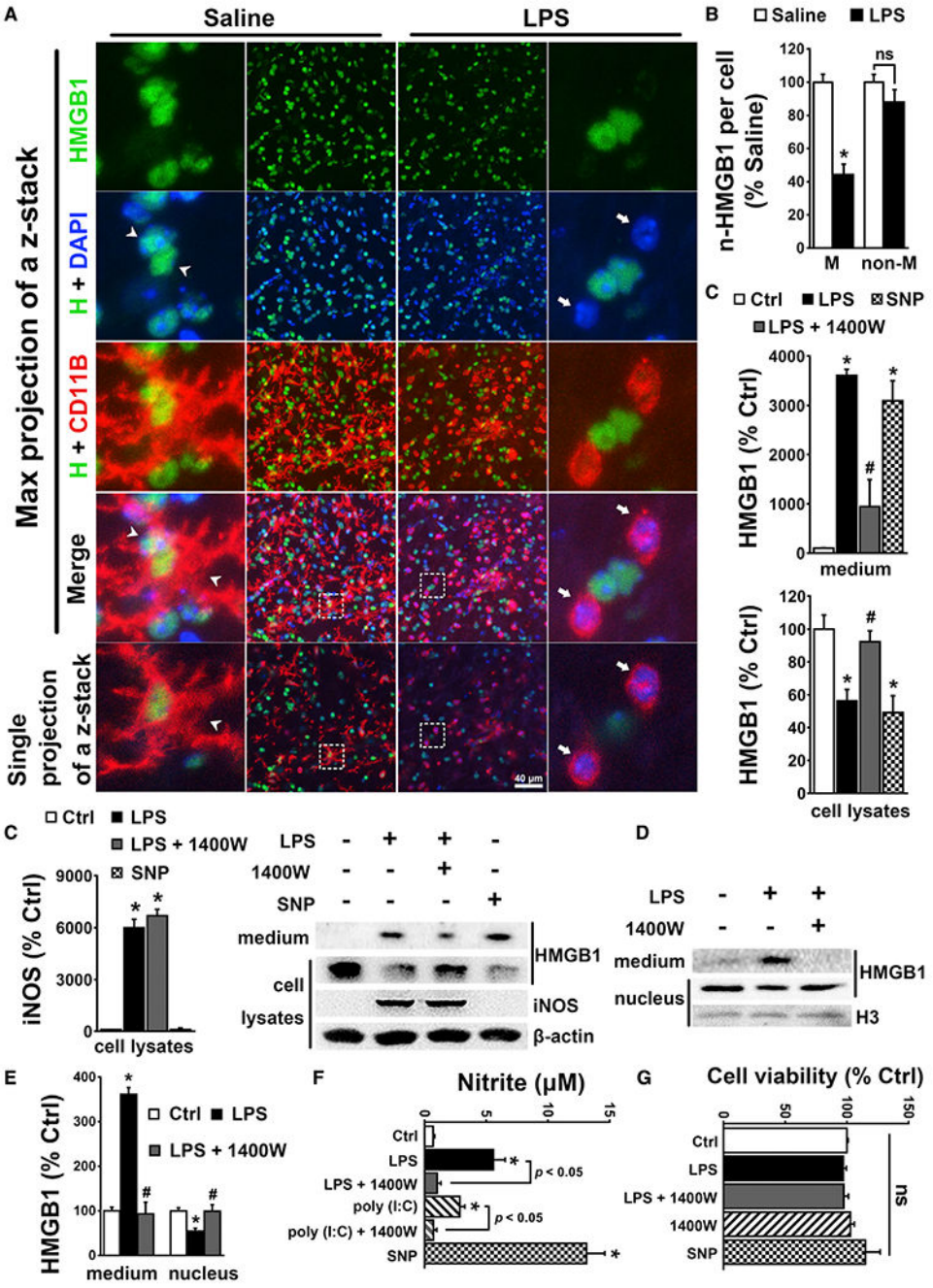

Figure 1. NO-mediated HMGB1 secretion from brain microglia/macrophages

(A and B) C57BL/6J mice received an intranigral injection of sterile normal saline (2 μL) or LPS(3 μg in 2 μL of saline; 1.8×10^3 endotoxin unit [EU]). At 24 h after the injection, representative confocal double-labeling fluorescence images showed active morphology of CD11b-IR microglia/macrophages (M) and reduction in nuclear HMGB1 (n-HMGB1) after LPS injection. Arrowheads show strong staining of n-HMGB1 in ramified (resting) microglia/macrophages in saline-injected SN. Arrows show faint n-HMGB1 in active microglia/macrophages with amoeboid-like morphology in LPS-injected SN. H, HMGB1

(A). Quantification of n-HMGB1 staining of the maximum intensity projection of a z stack of 30 confocal images from a brain slice taken at 1 mm step size, which displayed 3D structure in a 2D image. We measured 431 and 863 CD11b-IR microglia/macrophages (M) as well as 1,196 and 1,026 CD11b-negative and DAPI-positive non-microglia/macrophage cells (non-M) in saline- and LPS-injected SN, respectively. Fluorescence intensity of n-HMGB1 staining per cell was calculated and normalized to each respective saline-injected control. n = 3 mice for each group. *$p < 0.05$; unpaired two-tailed Student's t test (B).

(C) Microglia-enriched cultures were treated with LPS (15 ng/mL), NO donor SNP (20 μM), or vehicle with or without 30-min pretreatment with the iNOS inhibitor 1400W (10 μM). Immunoblotting and densitometry analysis showed the levels of HMGB1 and iNOS in whole-cell lysates and the levels of extracellular HMGB1 in the concentrated culture medium 24 h after the treatment. n = 4.

(D and E) Nuclear fractionation and immunoblotting analysis showed blockage of LPS-elicited HMGB1 secretion by 1400W at 24 h after LPS treatment of BV2 microglial cells. The nuclear marker histone H3 was examined to monitor loading errors of nuclear proteins (D). Densitometry quantification of HMGB1 level (E). n = 3.

(F) The level of nitrite (an indicator of NO production) in the culture medium was measured at 24 h after microglia-enriched cultures were treated with LPS, poly(I:C), or SNP with or without 1400W pretreatment for 30 min. n = 3.

(G) MTT assay revealed no cytotoxicity after microglial cultures were treated with LPS, SNP, and/or 1400W for 24 h. n = 3. *$p < 0.05$ compared with the corresponding control. $^{\#}p < 0.05$ compared with LPS-treated cultures; one-way ANOVA with Sidak's multiple comparisons (C, E, F) and one-way ANOVA with Dunnett's multiple comparisons test (G). Ctrl, control; ns, not significant.

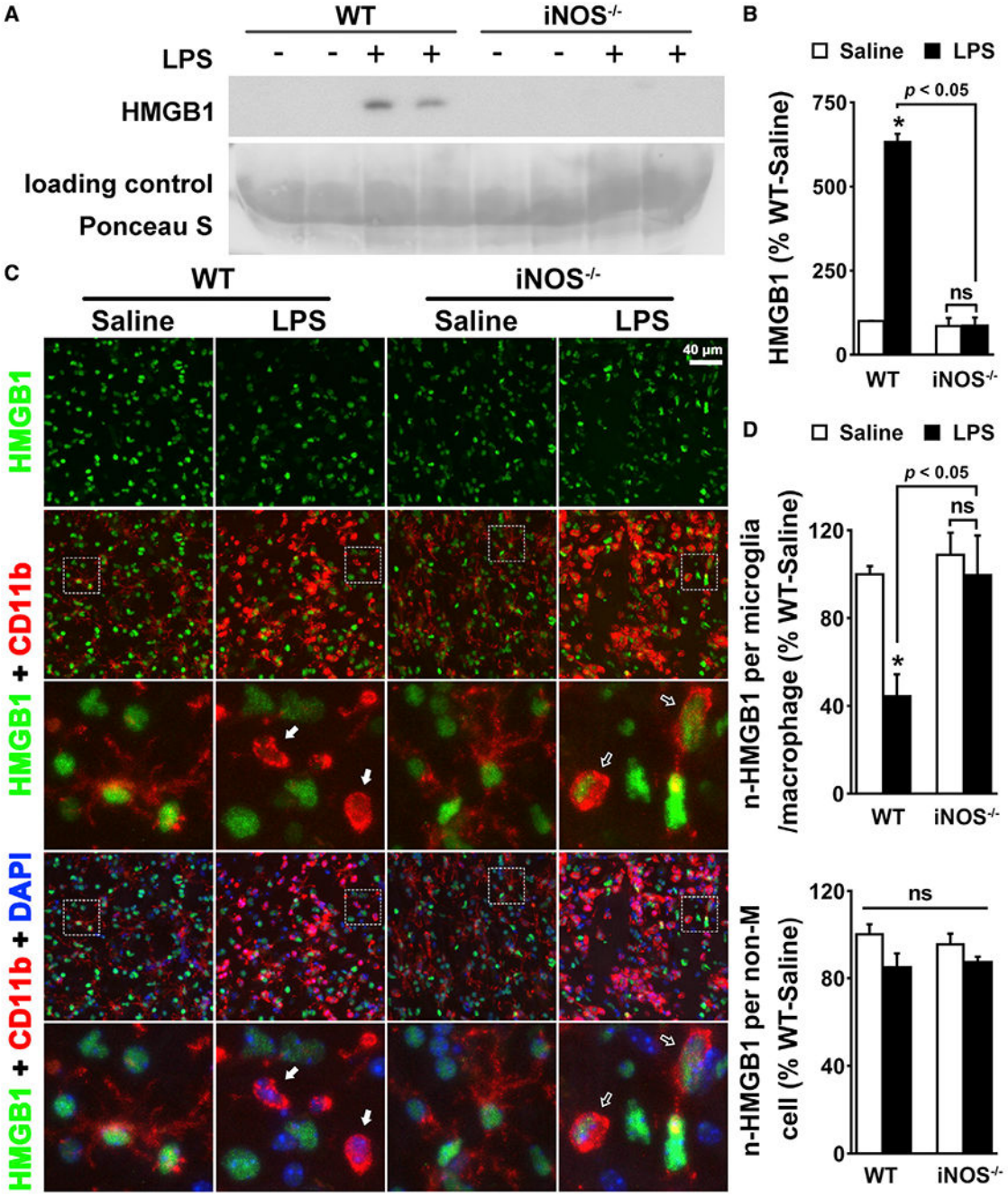

Figure 2. Genetic deletion of iNOS blocked LPS-induced HMGB1 secretion

(A and B) An i.p. injection of LPS (5 mg/kg; 3×10^6 EU/kg) increased serum HMGB1 in WT but not iNOS$^{-/-}$ mice at 5 h after LPS injection, as shown by immunoblotting (A) and densitometry quantification (B). n = 3 mice for each group.

(C and D) At 24 h after an intranigral injection of LPS, activated microglia/macrophages with amoeboid-like morphology in LPS-injected SN of WT mice showed faint n-HMGB1 staining. Activated microglia/macrophages in LPS-injected SN of iNOS$^{-/-}$ mice displayed strong n-HMGB1 staining, as resting microglia/macrophages in saline-injected SN of WT

and iNOS$^{-/-}$ mice did. White arrows indicate activated microglia/macrophages with faint n-HMGB1 staining in LPS-injected SN of WT mice. Unfilled arrows indicate activated microglia/macrophages with strong n-HMGB1 staining in LPS-injected SN of iNOS$^{-/-}$ mice (C). Quantification of fluorescence intensity of n-HMGB1 staining of the maximum intensity projection of a z stack (D) was done as described in the legend to Figure 1B. We measured 297, 637, 421, and 722 microglia/macrophages as well as 904, 1,230, 689, and 1,056 non-microglia/macrophage (non-M) cells for WT-saline, WT-LPS, iNOS$^{-/-}$-saline, and iNOS$^{-/-}$-LPS, respectively. Fluorescence intensity of n-HMGB1 staining per cell was calculated and normalized to each respective saline-injected WT control. n = 3 mice for each group. *$p < 0.05$ compared with the saline-injected control; two-way ANOVA with Tukey's multiple comparisons (B and D).

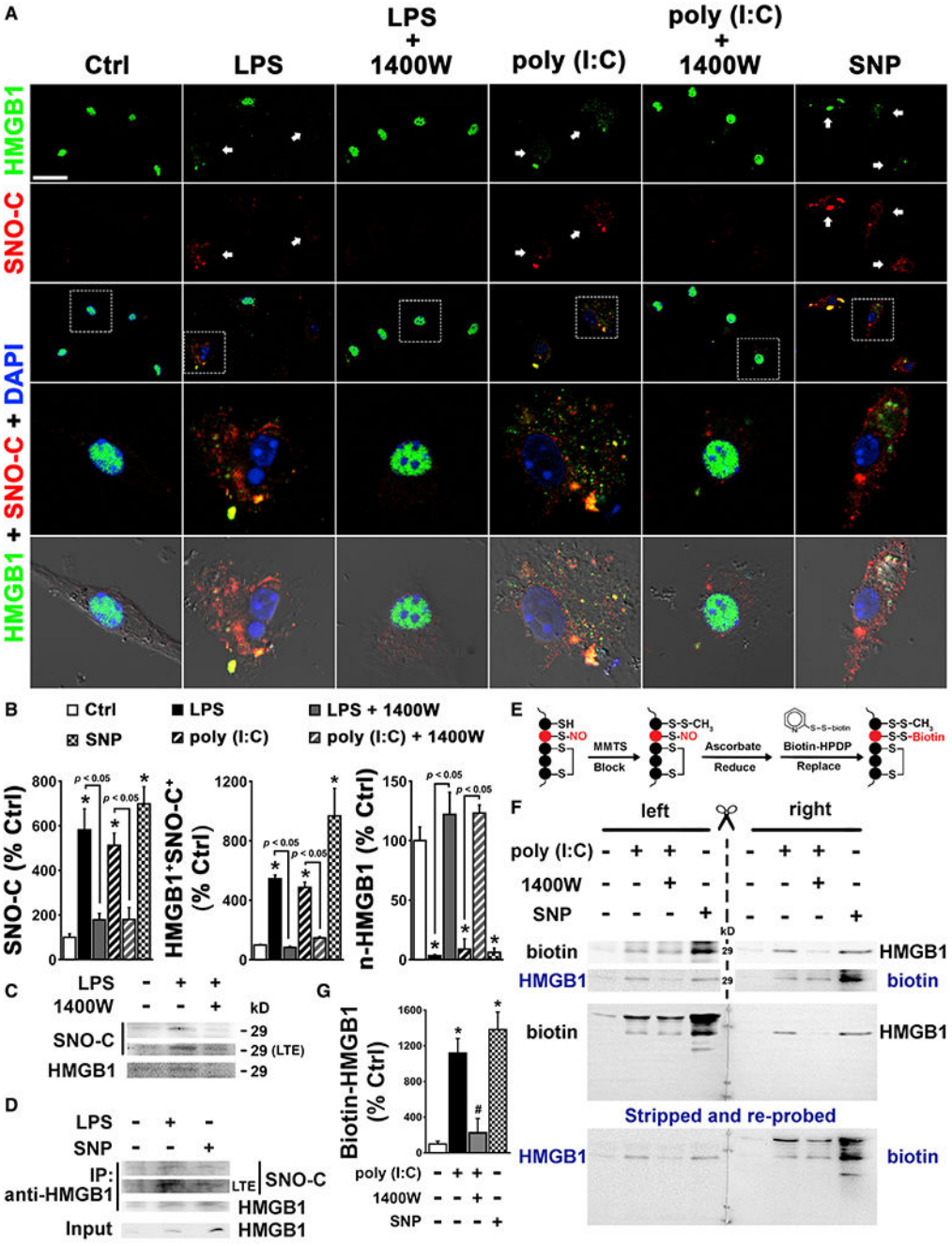

Figure 3. SNO modification induced nucleocytoplasmic shuttling and extracellular secretion of HMGB1

(A and B) Microglia-enriched cultures treated with LPS, poly(I:C), or SNP showed S-nitroso-cysteine (SNO-C) and SNO-C^{+}HMGB1^{+} staining in the cytosol as well as faint n-HMGB1 staining that was negative for SNO-C. Blockage of NO production with 1400W prevented LPS- and poly(I:C)-induced occurrence of cytosolic SNO-C^{+}HMGB1^{+} staining and reduction in n-HMGB1 (A). Quantification of fluorescence intensity of SNO-C (B). n = 3. Scale bar: 30 μm.

(C) Immunoblotting analysis, in which separated proteins were immunoblotted and probed for SNO-C and, after the blotting membrane was stripped, for HMGB1, showed that secreted HMGB1 in the concentrated medium of microglia-enriched cultures was S-nitrosylated after LPS treatment. 1400W attenuated LPS-elicited secretion of SNO-HMGB1. LTE, long time exposure; n = 4.

(D) Immunoprecipitation (IP) using anti-HMGB1 antibody indicated that immunoprecipitated HMGB1 from the concentrated medium of LPS- or SNP-treated BV2 microglial cells was positive for SNO-C. LTE, long time exposure; n = 3.

(E) Schematic diagram of the principle and the procedure of the biotin-switch assay illustrated by a theoretical protein with cysteines in the free thiol, disulfide, or nitrosothiol conformation.

(F and G) RAW 264.7 cell cultures were treated with vehicle, poly(I:C), or SNP in serum-free DMEM for 24 h. Following the biotin-switch assay, biotinylated supernatant proteins were separated by non-reducing SDS-PAGE (no boiling and no reducing agent β-mercaptoethanol or DTT in the sample buffer) and transferred to polyvinylidene fluoride (PVDF) membranes. The same protein samples were loaded to one SDS-PAGE gel twice with the prestained protein marker in between. Separated proteins that contained biotinylated cysteines were immunoblotted and probed for biotin using mouse monoclonal anti-biotin antibody and, after the membrane was stripped, for HMGB1 using rabbit polyclonal anti-HMGB1 antibody or vice versa (F). Densitometry values of HMGB1 were normalized to those of vehicle-treated control. The secreted HMGB1 from poly(I:C)- or SNP-treated RAW 264.7 cells was biotinylated (i.e., originally S-nitrosylated). Pretreatment with 1400W blocked poly(I:C)-elicited SNO modification and secretion of HMGB1 (G). n = 3. Significance was determined by one-way ANOVA with Sidak's multiple comparisons. *$p < 0.05$ compared with vehicle-treated controls. $^{\#}p < 0.05$ compared with the corresponding LPS- or poly(I:C)-treated cultures.

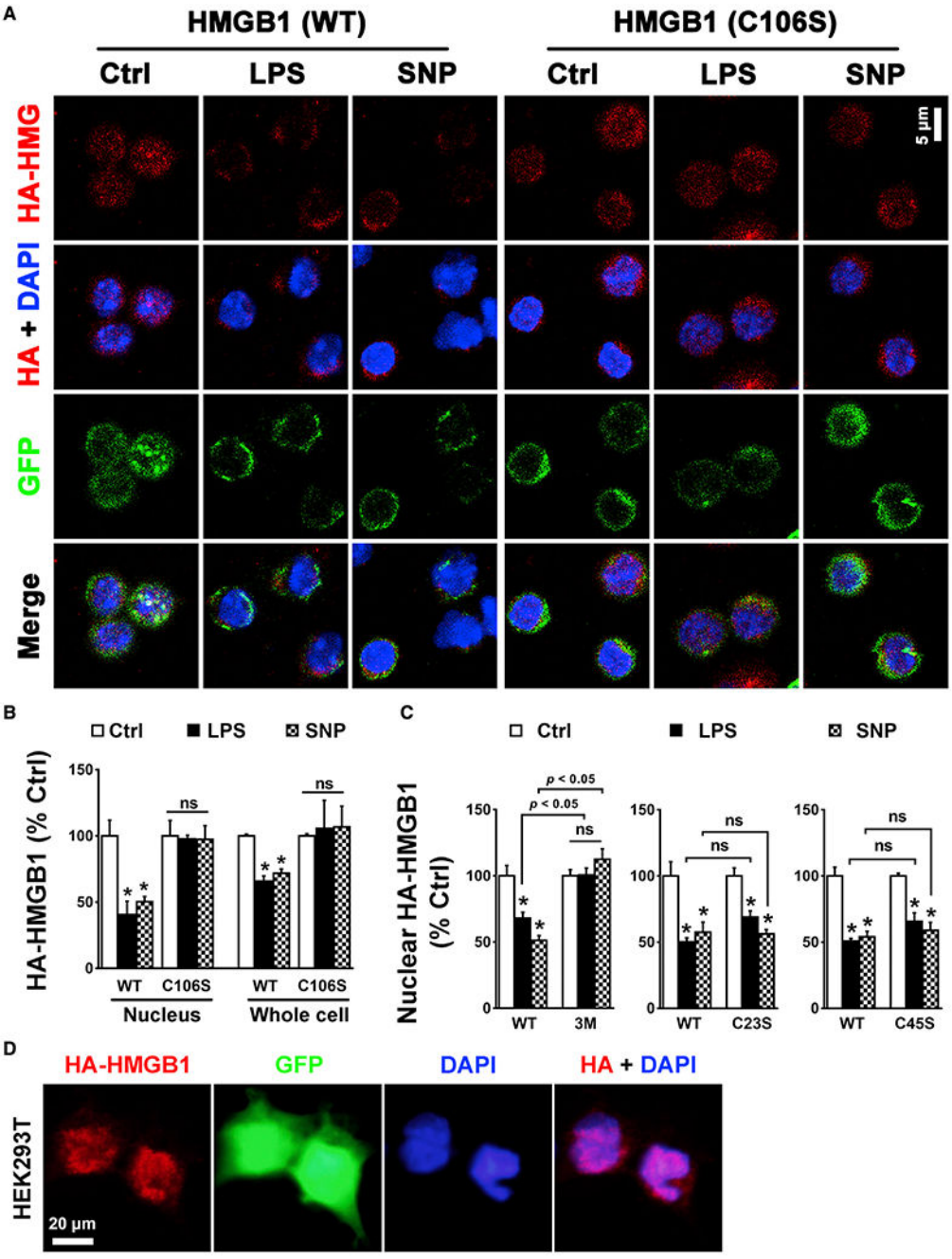

Figure 4. SNO modification of HMGB1 at Cys106 was required for its secretion

Mouse peritoneal macrophages (A–C and Figure S2) transfected with plasmids pCS2(+)-4HA-HMGB1 and pLVX-GFP were treated with vehicle, LPS, or SNP for 24 h. (A) Representative images show LPS- or SNP-elicited nucleus-to-cytoplasm shuttling of WT HA-HMGB1 but not C106S mutant HA-HMGB1, as indicated by the treatment-elicited distinctive staining pattern change of HA-HMGB1 (WT) from nuclear staining in vehicle-treated macrophages to ring-like cytosolic staining in LPS- or SNP-treated macrophages and the nuclear retention of HA-HMGB1 (C106S) after vehicle, LPS, or SNP treatment. n = 3.

(B and C) The mean nuclear and total intracellular HA-HMGB1 intensity per cell was analyzed by ImageJ. C106S mutation (B) and C23SC45SC106S mutations (3M) (C) blocked LPS- and SNP-elicited HA-HMGB1 secretion. C23S or C45S mutation (C) did not significantly affect LPS- or SNP-triggered HA-HMGB1 secretion. n = 3. *$p < 0.05$ compared with the corresponding vehicle-treated control; two-way ANOVA with Sidak's multiple comparisons. Representative images of the effects of C23SC45SC106S, C23S, or C45S mutation on HA-HMGB1 nucleus-to-cytoplasm shuttling and secretion are presented in the Figure S2.

(D) HEK293T cells were transfected with plasmids pCS2(+)-4HA-HMGB1 (WT) and pLVX-GFP as a positive control for the plasmid transfection in macrophages. Like peritoneal macrophages, HEK293T cells exhibited nuclear location of WT HA-HMGB1. Different from its cytoplasmic location in peritoneal macrophages, GFP was distributed throughout HEK293T cells, which might result from passive penetration of overexpressed GFP (27 kDa) into the nuclei through nuclear pores, since GFP does not contain an NLS. Notably, different resistances of immune cells and non-immune cells to plasmid transfection led to a remarkable difference in the abundance of GFP or HA-HMGB1 expressed in macrophages and HEK293T cells. n = 3.

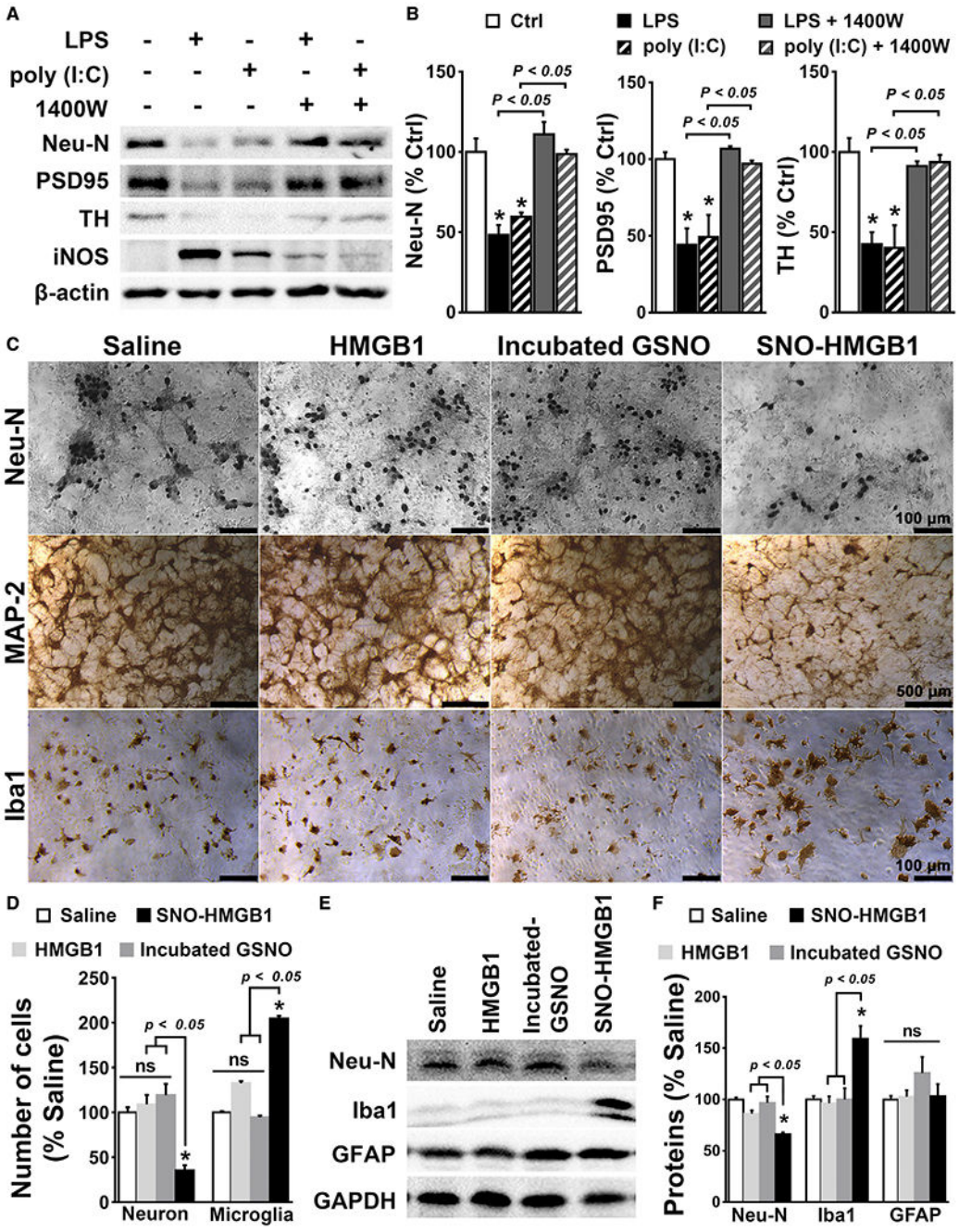

Figure 5. SNO-HMGB1 induced more profound microglial activation and neurodegeneration than unmodified HMGB1

(A and B) Midbrain neuron-glia cultures were treated with vehicle, 15 ng/mL LPS, or 50 μg/mL poly(I:C) for 7 days with or without pretreatment for 30 min with 10 μM 1400W. Immunoblotting analyses of levels of Neu-N, PSD95, TH, and iNOS were performed to evaluate neurodegeneration and neuroinflammation (A). Quantification of indicated proteins (B). n = 3.

(C–F) Midbrain neuron-glia cultures were treated with vehicle, unmodified HMGB1, or SNO-HMGB1 (250 ng/mL) or "incubated GSNO" (≤5 μM, as described under STAR

Methods) for 7 days. Immunocytochemistry (C and D) and immunoblot (E and F) show significant neurodegeneration and microglial activation in the cultures treated with SNO-HMGB1 but not other reagents. n = 3. *p < 0.05 compared with the corresponding saline-treated control; one-way ANOVA with Sidak's multiple comparisons test.

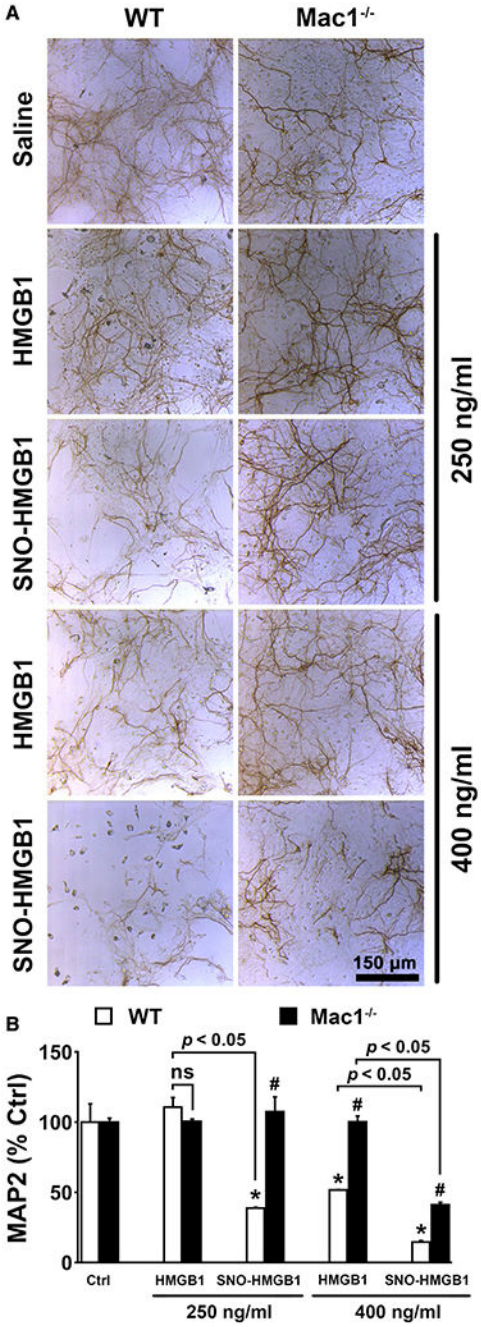

Figure 6. SNO-HMGB1 induced more profound neurodegeneration in WT neuron-glia cultures than in Mac1$^{-/-}$ cultures

(A and B) Midbrain neuron-glia cultures prepared from WT or Mac1$^{-/-}$ mice were treated with vehicle, unmodified HMGB1, or SNO-HMGB1 for 7 days. Immunocytochemistry for MAP-2 and densitometry analysis showed that Mac1$^{-/-}$ cultures were more resistant to unmodified HMGB1 and SNO-HMGB1 than WT cultures (A). Densitometry analysis of MAP2 (B). n = 3. *p < 0.05 compared with the corresponding saline-treated control. $^{\#}$p < 0.05 compared with the corresponding WT cultures; two-way ANOVA with Sidak's multiple comparisons.

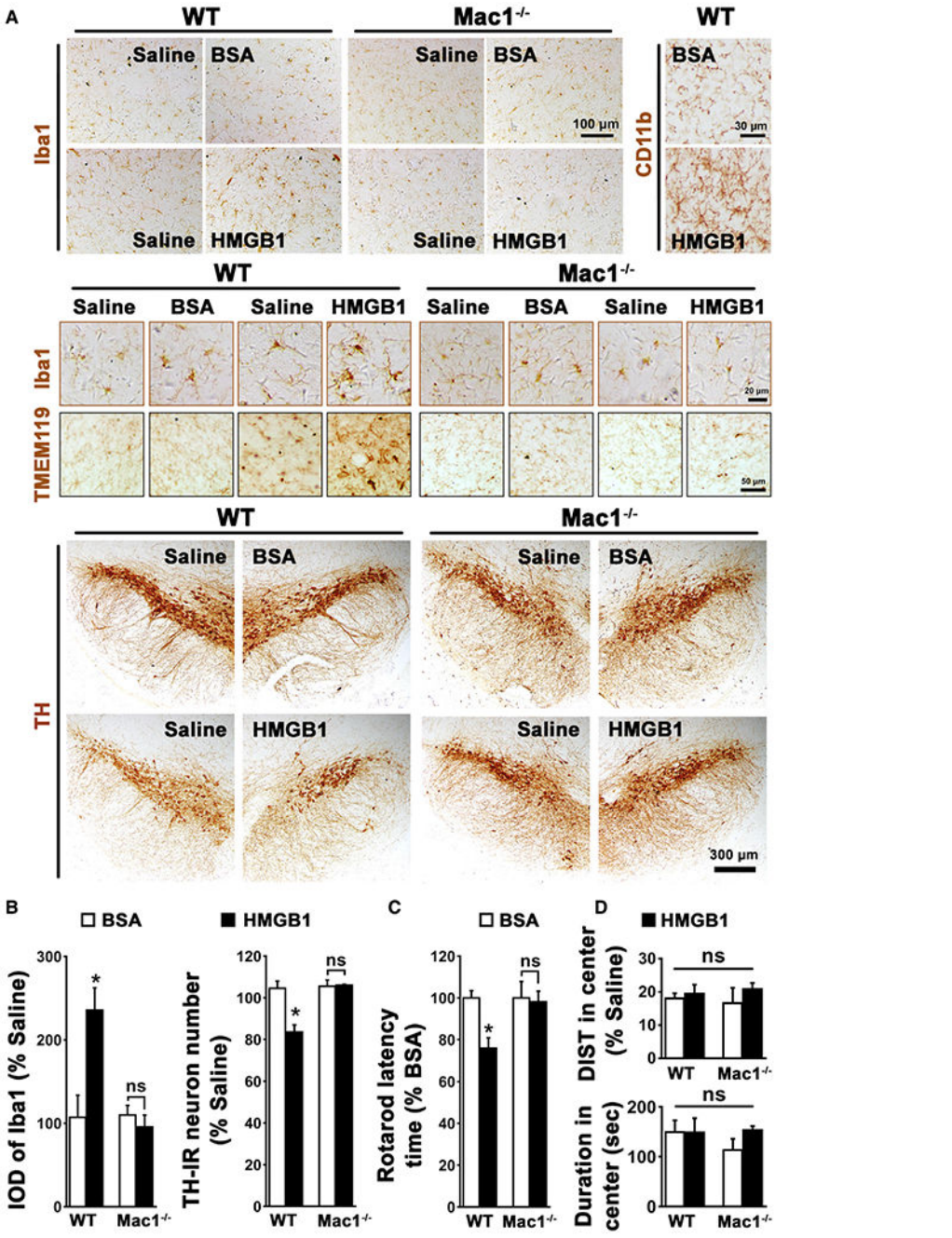

Figure 7. Intranigral HMGB1 injection induced chronic microglial activation, dopaminergic neurodegeneration, and locomotor deficit in WT but not Mac1$^{-/-}$ mice

Mac1$^{-/-}$ and WT (C57BL/6) mice received an intranigral injection of endotoxin-free HMGB1 (2 μg) or BSA (2 μg; as a control). One month later, PD-like phenotypes were examined.

(A and B) HMGB1-elicited nigral microglia/macrophage activation was shown by elevated immunoreactivity of Iba1, CD11b, and TMEM119; enlarged size; and irregular shape in WT mice but not Mac1$^{-/-}$ mice. Decreased number of TH-IR neurons and damaged integrity of TH-IR fibers indicated HMGB1-elicited dopaminergic neurodegeneration only in WT

mice (A). Eight and four evenly spaced brain sections from a series of 24 sections that covered the entire SN were used for the count of TH-IR neurons and the measurement of the optical density of Iba1 immunoreactivity in nigral microglia/macrophages, respectively, by two individuals blind to the treatment (B). n = 3 mice for each group.

(C) The rotarod behavior test showed HMGB1-elicited impairment of locomotor activity in WT mice but not $Mac1^{-/-}$ mice. n = 5 mice for each group.

(D) The open field test did not show alteration in exploratory activity or anxiety-related activities in HMGB1- or BSA-injected WT or Mac1−/− mice. n = 5 mice for each group.

*$p < 0.05$ compared with BSA-injected controls; two-way ANOVA with Tukey's multiple comparisons.

KEY RESOURCES TABLE

REAGENT or RESOURCE	SOURCE	IDENTIFIER
Antibodies		
Rabbit monoclonal anti-β-Actin (D6A8)	Cell Signaling Technology	Cat# 8457; RRID:AB_10950489
Mouse monoclonal anti-Biotin (33)	Santa Cruz Biotechnology	Cat# sc-101339; RRID:AB_1119609
Rat monoclonal anti-CD11b	Bio-Rad Laboratories	Cat# MCA711G; RRID:AB_323167
Rabbit monoclonal anti-GAPDH (14C10)	Cell Signaling Technology	Cat# 2118; RRID: AB_561053
Mouse monoclonal anti-GFAP	Santa Cruz Biotechnology	Cat# sc-65343; RRID:AB_783553
Rabbit polyclonal anti-GFAP	Agilent	Cat# Z0334; RRID:AB_10013382
Mouse monoclonal anti-GFP	Beyotime	Cat# AF0159
Rabbit polyclonal anti-H3 (K4)	Bioworld	Cat# BS1174; RRID:AB_1663967
Rabbit monoclonal anti-HA	Cell Signaling Technology	Cat# 3724; RRID:AB_1549585
Rabbit polyclonal anti-HMGB1	Abcam	Cat# ab18256; RRID:AB_444360
Rabbit polyclonal anti-Iba1	Wako	Cat# 019-19741; RRID:AB_839504
Rabbit monoclonal anti-iNOS	Cell Signaling Technology	Cat# 13120; RRID:AB_2687529
Mouse monoclonal anti-MAP2	Millipore	Cat# MAB3418; RRID:AB_94856
Mouse monoclonal anti-NeuN	Sigma/Merck/Millipore	Cat# MAB377; RRID:AB_2298772
Mouse monoclonal anti-PSD95	Millipore	Cat# MABN68; RRID:AB_10807979
Mouse monoclonal anti-S-nitrosocysteine	Abcam	Cat# ab94930; RRID:AB_10697568
Rabbit polyclonal anti- Tyrosine Hydroxylase (TH)	Millipore	Cat# AB152; RRID:AB_390204
Mouse monoclonal anti-TH	Sigma-Aldrich	Cat# T2928; RRID:AB_477569
Mouse monoclonal anti-TMEM119	Synaptic Systems	Cat# 400 011; RRID:AB_2782984
Horse Anti-mouse IgG, HRP-linked Antibody	Cell Signaling Technology	Cat# 7076; RRID:AB_330924
Goat anti-rabbit IgG, HRP-linked Antibody	Cell Signaling Technology	Cat# 7074; RRID:AB_2099233
Goat anti-Mouse IgG (H+L) Highly Cross-Adsorbed Secondary Antibody, Alexa Fluor 488	Thermo Fisher Scientific	Cat# A-11029, RRID:AB_2534088
Goat anti-Mouse IgG (H+L) Highly Cross-Adsorbed Secondary Antibody, Alexa Fluor 594	Thermo Fisher Scientific	Cat# A-11032; RRID:AB_2534091
Goat anti-Rabbit IgG (H+L) Highly Cross-Adsorbed Secondary Antibody, Alexa Fluor 488	Thermo Fisher Scientific	Cat# A-11034; RRID:AB_2576217
Goat anti-Rabbit IgG (H+L) Highly Cross-Adsorbed Secondary Antibody, Alexa Fluor 594	Thermo Fisher Scientific	Cat# A-11037; RRID:AB_2534095
Goat anti-Rat IgG (H+L) Cross-Adsorbed Secondary Antibody, Alexa Fluor 594	Thermo Fisher Scientific	Cat# A-11007; RRID:AB_10561522
Chemicals, peptides, and recombinant proteins		
cOmplete™, EDTA-free Protease inhibitor cocktail tablets	Roche	Cat# 11873580001
ECL Western Blotting Detection Reagents	GE Healthcare	Cat# RPN2106
Lipopolysaccharide (LPS, E. coli O111: B4)	Calbiochem	Cat# 437627

REAGENT or RESOURCE	SOURCE	IDENTIFIER
LPS (Escherichia coli 0111:B4)	Sigma-Aldrich	Cat# L3012
Poly (I:C) (γ-irradiated)	Sigma-Aldrich	Cat# P0913
Recombinant Mouse HMGB1 (carrier-free)	Biolegend	Cat# 764006
Sodium nitroprusside dehydrate (SNP)	Sigma-Aldrich	Cat# 71778
S-Nitrosoglutathione (GSNO)	Sigma-Aldrich	Cat# N4148
1400W	Sigma-Aldrich	Cat# W4262
1400W 2HCl	Selleck	Cat# S8337
LipoMax™ Transfection Reagent	SUDGEN	Cat# 32010
ABC kit	Vectastain	Cat# PK-6100
Opti-MEM® reduced serum medium	Thermo Fisher Scientific	Cat# 31985070
Superscript III First-Strand Synthesis System	Thermo Fisher Scientific	Cat# 18080-051
EN-Link™ HPDP-Biotin	Thermo Fisher Scientific	Cat# 21341
Dulbecco's Modified Eagle's Medium (DMEM)	ATCC	Cat# 30-2002
DMEM/F-12, HEPES	Thermo Fisher Scientific	Cat# 11330-032/11330-057
RPMI 1640, no glutamine	Thermo Fisher Scientific	Cat# 21870-076
MEM, no glutamine	Thermo Fisher Scientific	Cat# 11090081/11090-099
Gibco™ Fetal Bovine Serum, certified	Thermo Fisher Scientific	Cat# 16000-044
L-Glutamine (200 mM)	Thermo Fisher Scientific	Cat# 25030-149
Sodium Pyruvate (100 mM)	Thermo Fisher Scientific	Cat# 11360-070
MEM Non-Essential Amino Acids Solution (100X)	Thermo Fisher Scientific	Cat# 11140-050
Penicillin-Streptomycin (10,000 U/mL)	Thermo Fisher Scientific	Cat# 15140-148
S-Methyl methanethiosulfonate	Sigma-Aldrich	Cat# 208795
Phanta® Max Super-Fidelity DNA Polymerase	Vazyme	Cat# P505
Critical commercial assays		
TIANprep Mini Plasmid Kit	TIANGEN	Cat# DP103
ClonExpress® II One Step Cloning Kit	Vazyme	Cat# C112
Mut Express® II Fast Mutagenesis Kit V2	Vazyme	Cat# C214
Deposited data		
Raw immunoblotting images	This paper	https://dx.doi:10.17632/zxs62xh37z.1
Experimental models: Cell lines		
BV2 microglial cell lines	Gao et al., 2003	N/A
RAW 264.7	Zhou et al., 2013	ATCC Cat# TIB-71, RRID:CVCL_0493
Experimental models: Organisms/strains		
Mouse: C57BL/6J	Jackson Laboratory	Stock# 000664
Mouse: B6.129P2-Nos2tm1Lau/J	Jackson Laboratory	Stock# 002609
Mouse: B6.129S4–Itgamtm1Myd/J ($Mac1^{-/-}$)	Jackson Laboratory	Stock# 003991
Mouse: B6.129S6–Cybbtm1Din/J ($gp91^{-/-}$)	Jackson Laboratory	Stock# 002365
Mouse: C57BL/6	Gempharmatech	Cat# N000013

REAGENT or RESOURCE	SOURCE	IDENTIFIER
Oligonucleotides		
WT HMGB1 fragment Forward PCR primer, ggagaaacttcagaccggacg	This study	N/A
WT HMGB1 fragment Reverse PCR primer, gggctatctaaagacacattcgg	This study	N/A
pCS2(+)-4HA-HMGB1 Forward PCR primer, tacgctggccggcctgaattcggcaaaggagatcctaaaaagccga	This study	N/A
pCS2(+)-4HA-HMGB1 Reverse PCR primer, gctatctagtcatgaagatctctgcgctagaaccaacttattcatc	This study	N/A
pCS2(+)-4HA-HMGB1 C23S-XhoI mutant Forward PCR primer, gtgcaaacctcgagggaggagcacaagaagaagcac	This study	N/A
pCS2(+)-4HA-HMGB1 C23S-XhoI mutant Reverse PCR primer, ctcctccctcgaggtttgcacaaagaatgcatatgaggacat	This study	N/A
pCS2(+)-4HA-HMGB1 C45S mutant Forward PCR primer, tccaagaagtcctcagagaggtggaagaccatgtctg	This study	N/A
pCS2(+)-4HA-HMGB1 C45S mutant Reverse PCR primer, cctctctgaggacttcttggagaactctgagaagttgacag	This study	N/A
pCS2(+)-4HA-HMGB1 C106S mutant Forward PCR primer, ttcttgttctcttctgagtaccgccccaaaatcaaag	This study	N/A
pCS2(+)-4HA-HMGB1 C106S mutant Reverse PCR primer, gtactcagaagagaacaagaagaaggccgaaggagg	This study	N/A
Recombinant DNA		
pCS2(+)-4HA plasmid	Gift from Dr. Zhen Zhu (Nanjing University)	N/A
pLVX-GFP	Gift from Dr. Geng Liu (Nanjing University)	N/A
Software and algorithms		
GraphPad Prism 7	GraphPad Software, Inc.	https://www.graphpad.com/scientific-software/; RRID:SCR_002798
Black Zen software (Zeiss LSM880)	Carl Zeiss	https://www.zeiss.com/microscopy/us/products/confocal-microscopes.html; RRID:SCR_018163
ImageJ	NIH	https://imagej.nih.gov/ij/